Chinese Journal of Natural Medicines

Dual targeting of cutaneous inflammation and vasculopathy *via* STING–NF–κB blockade underlies the anti–psoriatic efficacy of Yinxie Granules

Jueyao Zou, Tongyao Hu, Zhengyu Zhang, Yong He, Yuxin Wang, Yixiao Zhou, Ziyan Zhu, Suyun Yu, Wei Zou, Zhonghong Wei, Yang Zhao, Yanhong Pan, Wenxing Chen, Yin Lu

Citation: Jueyao Zou, Tongyao Hu, Zhengyu Zhang, Yong He, Yuxin Wang, Yixiao Zhou, Ziyan Zhu, Suyun Yu, Wei Zou, Zhonghong Wei, Yang Zhao, Yanhong Pan, Wenxing Chen, Yin Lu, Dual targeting of cutaneous inflammation and vasculopathy *via* STING–NF–κB blockade underlies the anti–psoriatic efficacy of Yinxie Granules, Chinese Journal of Natural Medicines, 2026, 24(7), 832–848. doi: 10.1016/S1875–5364(26)61112–0.

View online: https://doi.org/10.1016/S1875–5364(26)61112–0

Related articles that may interest you

Total glucosides of paeony alleviates cGAS–STING–mediated diseases by blocking the STING–IRF3 interaction

Chinese Journal of Natural Medicines. 2024, 22(5), 402–415 https://doi.org/10.1016/S1875–5364(24)60572–8

Five Rutaceae family ethanol extracts alleviate H_2O_2 and LPS–induced inflammation *via* NF–κB and JAK–STAT3 pathway in HaCaT cells

Chinese Journal of Natural Medicines. 2022, 20(12), 937–947 https://doi.org/10.1016/S1875–5364(22)60217–6

Esculetin protects against early sepsis *via* attenuating inflammation by inhibiting NF–κB and STAT1/STAT3 signaling

Chinese Journal of Natural Medicines. 2021, 19(6), 432–441 https://doi.org/10.1016/S1875–5364(21)60042–0

Cyasterone inhibits IL–1β–mediated apoptosis and inflammation *via* the NF–κB and MAPK signaling pathways in rat chondrocytes and ameliorates osteoarthritis *in vivo*

Chinese Journal of Natural Medicines. 2023, 21(2), 99–112 https://doi.org/10.1016/S1875–5364(23)60388–7

Yanggan Jiangmei Formula alleviates hepatic inflammation and lipid accumulation in non–alcoholic steatohepatitis by inhibiting the NF–κB/NLRP3 signaling pathway

Chinese Journal of Natural Medicines. 2024, 22(3), 224–234 https://doi.org/10.1016/S1875–5364(24)60595–9

The bioinformatics and metabolomics research on anti–hypoxic molecular mechanisms of Salidroside *via* regulating the PTEN mediated PI3K/Akt/NF–κB signaling pathway

Chinese Journal of Natural Medicines. 2021, 19(6), 442–453 https://doi.org/10.1016/S1875–5364(21)60043–2

Wechat

Chinese Journal of Natural Medicines 24 (2026) 832-848

Contents lists available at ScienceDirect

Chinese Journal of Natural Medicines

journal homepage: www.cjnmcpu.com/



Original article

Dual targeting of cutaneous inflammation and vasculopathy *via* STING-NF-κB blockade underlies the anti-psoriatic efficacy of Yinxie Granules

Jueyao Zou[a], Tongyao Hu[a], Zhengyu Zhang[a], Yong He[a], Yuxin Wang[a], Yixiao Zhou[a], Ziyan Zhu[a], Suyun Yu[a,b], Wei Zou[a], Zhonghong Wei[a], Yang Zhao[a,b], Yanhong Pan[a,b,*], Wenxing Chen[a,c,d,*], Yin Lu[a,c,d,*]

[a] *Jiangsu Key Laboratory for Pharmacology and Safety Research of Chinese Materia Medica, Nanjing University of Chinese Medicine, Nanjing 210023, China*
[b] *School of Medicine, Nanjing University of Chinese Medicine, Nanjing 210023, China*
[c] *Jiangsu Joint International Research Laboratory of Chinese Medicine and Regenerative Medicine, Nanjing 210023, China*
[d] *Jiangsu Collaborative Innovation Center of Traditional Chinese Medicine (TCM) Prevention and Treatment of Tumor, Nanjing 210023, China*

ARTICLE INFO

Article history:
Received 17 July 2025
Revised 15 September 2025
Accepted 20 November 2025
Available online 20 July 2026

Keywords:
Psoriasis
Yinxie Granules
STING-NF-κB
Skin inflammation
Vascular remodeling
STING inhibitor

ABSTRACT

Psoriasis is a chronic skin disease driven by skin inflammation and abnormal subcutaneous blood vessels. Yinxie Granules (YXKL) is a clinically effective traditional Chinese medicine (TCM) formula that has shown promise in psoriasis treatment, but its pharmacological mechanisms and material basis remain unclear, limiting its clinical application and co-administration with other drugs. In this study, we explored the mechanism and active components of YXKL in the treatment of psoriasis using patient samples, IMQ-induced psoriatic mice, zebrafish, and *in vitro* assays. We discovered that YXKL alleviated skin inflammation and restored the skin barrier by reducing M1 macrophage/Th17 infiltration, lowering pro-inflammatory cytokines (IL-6, IFN-β, IL-23, IL-17), and increasing loricrin expression. Mechanistically, we identified a dynamic transition in STING signaling during psoriasis progression. Both the STING/IRF3 and STING/NF-κB pathways were activated in moderate psoriasis, while only the STING/NF-κB pathway was hyperactivated in severe disease. YXKL specifically targeted the STING/NF-κB pathway to mitigate inflammation and vasculopathy but had no significant impact on the upstream regulators, including TRAF6, LKB1, AMPK, and ULK1. Quercetin and kaempferol were identified as the primary STING-modulating components in YXKL, binding to STING proteins and inhibiting downstream pathway activation. These flavonoid components mediate the anti-psoriatic effects of YXKL by simultaneously suppressing skin inflammation and angiogenesis while enhancing vascular integrity through STING inhibition in both keratinocytes and endothelial cells. Our results elucidated the molecular basis of YXKL for psoriasis treatment, highlighting STING/NF-κB as a pivotal therapeutic target in mitigating psoriasis development and providing natural candidate compounds as potential STING inhibitors.

1. Introduction

Psoriasis, a chronic inflammatory skin disorder linked to immune system dysfunction, is strongly associated with a spectrum of systemic comorbidities, including diabetes, cardiovascular disease, and depression, contributing to increased mortality and socioeconomic burden [1]. The current understanding of psoriasis pathogenesis largely centers around the interplay between the innate and adaptive immune systems and the amplification of psoriatic inflammation. Various immune cells release pro-inflammatory cytokines like TNF-α, IL-23, and IL-17. These cytokines stimulate keratinocyte hyperproliferation, differentiation, and inflammatory cytokine production, intensifying chronic inflammation and compromising the skin barrier in psoriasis, resulting in tissue inflammatory damage [2]. Research by Svedbom et al. [3] has demonstrated a correlation between psoriasis severity and systemic inflammation as well as cardiovascular disease. However, biologics targeting inflammatory cytokines have not met expectations, with some patients showing no response or even experiencing exacerbated symptoms [4-6].

Emerging evidence underscores the pivotal role of vascular endothelial cells (ECs) in psoriasis pathogenesis, where they actively contribute to skin inflammation and disease chronicity [7, 8]. Key mediators such as vascular endothelial growth factor (VEGF) trigger pathological angiogenesis, disrupt vascular barrier integrity, and induce severe psoriasis-like inflammation [9-11]. A specific subset of cutaneous ECs expressing insulin-like growth factor binding protein 7 (IGFBP7) damages the endothelial glycocalyx, increasing vascular permeability and facilitating immune cell infiltration [7]. Interactions among Wnt family member 5A $(WNT5A)^+$ fibroblasts, versican $(VCAN)^+$ vascular smooth muscle cells, and inter-alpha-trypsin inhibitor heavy chain 5 $(ITIH5)^+$ vascular ECs promote leukocyte recruitment and angiogenesis [12]. However, S-phase kinase-associated protein 2 (SKP2) knockout in ECs reduces angiogenesis and immune cell infiltration at psoriasis lesions [8]. Importantly, a vicious cycle develops where pro-inflam-

* Corresponding author.
E-mail addresses: yanhongpan@njucm.edu.cn (Y. Pan); chenwx@njucm.edu.cn (W. Chen); luyingreen@njucm.edu.cn (Y. Lu)

https://doi.org/10.1016/S1875-5364(26)61112-0
Copyright © 2026, China Pharmaceutical University. Published by Elsevier B.V. All rights are reserved.

matory cytokines from immune cells compromise endothelial barriers and promote angiogenesis, while activated ECs release factors that further amplify immune responses [13]. This crosstalk between vascular dysfunction and skin inflammation fuels the chronicity and refractory nature of psoriasis, highlighting the need for dual targeting of both inflammatory and vascular components for effective therapy.

The stimulator of interferon genes (STING), a crucial element in cytosolic DNA-sensing, has emerged as a significant player in psoriasis pathogenesis [14-16]. Elevated levels of cell-free DNA in the serum of severe psoriasis patients support its involvement [17]. Upon activation by dsDNA, cyclic GMP-AMP synthase (cGAS) produces 2',3'-cGAMP (cGAMP), which diffuses through intercellular gaps and amplifies STING-mediated inflammatory response [18]. Inflammatory cytokines impair the immunological tolerance of keratinocytes to cytosolic DNA and facilitate the formation of the STING-TBK1 complex [19]. In ECs, STING activation regulates T-cell adhesion and transendothelial migration *via* type 1 interferon [20], and is linked to pathological angiogenesis, increased endothelial permeability, and VEGF production [21, 22]. Collectively, these findings position STING as a key molecular bridge connecting keratinocytes, immune cells, and ECs in psoriasis development. However, the distinct contribution and dynamics of the STING/IRF3 and STING/NF-κB pathways during disease exacerbation remain unclear. Clarifying these mechanisms is essential to avoid unintended suppression of protective immunity or premature discontinuation of therapy.

Traditional Chinese medicine (TCM), known for its holistic approach and documented efficacy in managing chronic inflammatory conditions, offers a promising complementary option. Yinxie Granules (YXKL), a TCM formula composed of Rhizoma Smilacis Glabrae (Tu-Fu-Ling) and Smilacis Chinae Rhizoma (Ba Qia), has been clinically applied for over 60 years and is approved in China for psoriasis treatment [23]. YXKL is often combined with other psoriasis medications to boost therapeutic efficacy [24]. Previous studies have shown that extracts of Rhizoma Smilacis Glabrae and Smilacis Chinae Rhizoma can lower TNF-α and IL-6 levels [25, 26]. Total glucosides of Rhizoma Smilacis Glabrae have also been reported to exert a therapeutic effect on psoriasis by regulating Th17/Treg balance [27]. However, the unclear molecular mechanisms and material basis underlying the anti-psoriatic effects of YXKL have restricted its clinical application rate.

In this study, we uncover the STING/IRF3-to-STING/NF-κB transition during psoriasis development, where STING/IRF3 governs early-phase inflammation while STING/NF-κB drives chronic progression. Our findings demonstrate that YXKL exerts a sustained anti-psoriasis effect by inhibiting the activation of the STING-NF-κB signaling pathway, thereby alleviating skin inflammation and remodeling vascular structure and function. Beyond revealing the molecular mechanism and material basis of YXKL for psoriasis treatment, our study underscores the critical role of the STING/NF-κB pathway in modifying the chronic phase of this disease. Additionally, it expands the repertoire of plant-derived STING inhibitors for the treatment of psoriasis, offering new therapeutic options.

2. Materials and methods

2.1. Cell lines

Human keratinocyte cell line HaCaT (Cellcook, Guangzhou, China) was cultured in Minimum Essential Medium (MEM; SenBeiJia, Nanjing, China) supplemented with 10% fetal bovine serum (FBS; Vazyme, Nanjing, China), 1% MEM non-essential amino acid (Gibico, USA, 11140050), and 1% penicillin/streptomycin (SenBeiJia, Nanjing, China). Human monocytic leukemia cell line THP-1 (Pricella, Wuhan, China) and human umbilical vein endothelial cells (HUVECs; Cellcook, Guangzhou, China) were maintained in Roswell Park Memorial Institute (RPMI) 1640 medium (Gibico, USA) and modified Dulbecco's Modified Eagle's Medium (DMEM; Cellcook, Guangzhou, China), respectively, both containing 10% FBS and 1% penicillin/streptomycin. Peripheral blood mononuclear cells (PBMCs; ORiCells, Shanghai, China, PB003F-C-5M) were utilized immediately following resuscitation.

To investigate the anti-inflammatory effects of quercetin (Aladdin, Shanghai, China, Q111273) and kaempferol (Aladdin, Shanghai, China, K107144), PMA (phorbol 12-myristate 13-acetate; MULTI SCIENCES, Hangzhou, China, 70-CS0001)-stimulated THP-1 cells were treated with LPS (Sigma, USA, L2880, 100 $ng \cdot mL^{-1}$) for 24 h, in the presence or absence of 10 $\mu mol \cdot L^{-1}$ of these compounds. Quercetin and kaempferol were dissolved in DMSO. To screen the inhibitory effects on the STING pathway, THP-1 cells were treated with these compounds for 2 h, then co-incubated with cGAMP (10 $\mu g \cdot mL^{-1}$; MCE, USA, HY-100564) and FuGENE 6 transfection reagent (Promega, USA, E2691) for 12 h. For *in vitro* psoriasis models, HaCaT cells, PBMCs, and HUVECs were stimulated with imiquimod (IMQ, 5 $\mu g \cdot mL^{-1}$; Shanghai Yuanye Bio-Technology Co., Ltd, China, S81181) or M5 [a mixture of IMQ (5 $\mu g \cdot mL^{-1}$), IFN-β (10 $ng \cdot mL^{-1}$; Peprotech, USA, AF-300-02B-5), IL-6 (10 $ng \cdot mL^{-1}$; Primegene, Shanghai, China, 101-06), IL-17 (10 $ng \cdot mL^{-1}$; Primegene, Shanghai, China, 101-07), and TNF-α (10 $ng \cdot mL^{-1}$; Primegene, Shanghai, China, 103-01)] for 24 h, with or without 10 $\mu mol \cdot L^{-1}$ kaempferol or quercetin.

2.2. IMQ-induced psoriatic murine model

BALB/c female mice (56–62 days old) were purchased from Vitonglihua Laboratory Animal Technology Co., Ltd. (Beijing, China). The housing and treatment of the mice were approved by the Ethical Committee for Animal Experiments of the Nanjing University of Chinese Medicine (Nos. 202304A011 and 202509A012). Mice were randomly divided into a control group, a model group, a 1.82 $g \cdot kg^{-1}$ YXKL [Rongchang Pharmaceuticals (ZIBO), Ltd., Shandong, China, dissolved in saline] group, and a 3.64 $g \cdot kg^{-1}$ YXKL group. Each group consisted of 18 mice. Before modeling, Veet hair removal cream was applied to the back skin of the mice to depilate an area of 2 cm × 3 cm. Two days later, 5% IMQ cream (SICHUAN MED-SHINE Pharmaceutical Co., Ltd., Sichuan, China, 62.5 mg per mouse) was applied to the right ear and back of the mice for modeling, once daily. The application ratio of the right ear to the back was 1∶4. Concurrently with modeling, gavage administration was initiated and performed twice daily at a dose of 0.1 mL/10 g. Both the control and model groups received an equal volume of saline. The back skin was photographed daily using a smartphone. The thickness of the right ear, psoriasis area, and severity index (PASI) score [14], and body weight were measured daily. On days 3, 5, and 7 after modeling and administration, 6 mice from each group were randomly selected and euthanized to collect the back skin and right ear. Additionally, images of subcutaneous blood vessels in the back skin were captured during tissue collection.

2.3. Histological analysis

The back skin and right ear of mice were fixed with 4% paraformaldehyde, dehydrated by ethanol gradient, paraffin-embedded, then sectioned (5 μm), and stained with hematoxylin-eosin (HE). The images were captured by the Mantra Pathology Workstation (PerkinElmer, Waltham, USA). The epidermal thickness of the dorsal skin and the right ear was quantified by Photoshop CS6 software (Adobe, USA). All histological assessments were performed in a blinded manner. The samples were coded by an independent researcher and analyzed by another researcher who was

blinded to the group assignments.

2.4. RNA extraction and real-time PCR

Total RNA was extracted from skin lesional samples and cells using TRIzol reagent (Vazyme, Nanjing, China, R401-01). The extracted RNA was then reverse transcribed into cDNA using Hiscript II Q RT SuperMix (Vazyme, Nanjing, China, R223-01). Quantitative PCR reactions were subsequently carried out using ChamQ SYBR qPCR Master Mix (Vazyme, Nanjing, China, Q331) on an ABI 7500 system (Applied Biosystems, CA, USA). GAPDH served as the reference gene, and the relative gene expression levels were quantified by applying the $2^{-\Delta\Delta Ct}$ method. The primer sequences are provided in Table S1.

2.5. Immunofluorescence

In brief, the tissue sections were deparaffinized, rehydrated, antigenically repaired, and incubated with 3% H_2O_2 to block endogenous peroxidase. After blocking with 5% bovine serum albumin (BSA), the samples were incubated with the primary antibody at 4 °C overnight. The primary antibodies were as follows: loricrin (1∶50, ABclonal, Wuhan, China, A21039), filaggrin (1∶200, ABclonal, Wuhan, China, A20011), F4/80 (1∶2000, Servicebio, Wuhan, China, GB113373), CD4 (1∶200, Servicebio, Wuhan, China, GB15064), IL-17 (1∶200, ABclonal, Wuhan, China, A12454), CD86 (1∶2000, Servicebio, Wuhan, China, GB115630), CD206 (1∶400, Servicebio, Wuhan, China, GB113497), CD31 (1∶200, Servicebio, Wuhan, China, GB11315), ZO-1 (1∶200, CST, USA, 13663S), VE-cadherin (1∶200, CST, USA, 2500S), STING (1∶200, Proteintech, Wuhan, China, 19851-1-AP), α-SMA (1∶200, CST, USA, 19245). The section was incubated with an HRP-conjugated secondary antibody (1∶300, Servicebio, Wuhan, China, GB233030) followed by amplification with iF555-Tyramide (1∶500, Servicebio, Wuhan, China, G1233), iF488-tyramide (1∶500, Servicebio, Wuhan, China, G1231), or CY3-tyramide (1∶500, Servicebio, Wuhan, China, G1223), or directly incubated with a Cy5-conjugated secondary antibody (1∶400, Servicebio, Wuhan, China, GB27303), Cy3-conjugated secondary antibody (1∶300, Servicebio, Wuhan, China, GB21303), or Alexa Fluor 488 labeled secondary antibody (1∶400, Servicebio, Wuhan, China, GB25301). For multicolor fluorescence staining, sections were subjected to antigen retrieval again before incubation with another primary antibody. Nuclei were stained with DAPI (Servicebio, Wuhan, China, G1012). Sections stained for F4/80, CD86, and CD206 were scanned using Pannoramic MIDl (3DHISTECH, Hungary), while the remaining sections were imaged with a Zeiss microscope (Zeiss Axio vert A1, Oberkochen, Germany). The images were analyzed by ImageJ software (National Institutes of Health, USA). The samples were coded by an independent researcher and analyzed by another researcher who was blinded to the group assignments.

2.6. Bioinformatic analysis

The mRNA expressions of STING and related genes in the skin and PBMCs of normal and psoriasis patients were obtained from the NCBI GEO portal (Accession numbers: GSE78097, GSE192867, and GSE67853) [28-30]. The ingredients contained in YXKL, along with their properties such as oral bioavailability (OB), drug-likeness (DL), and their targets, were sourced from the TCMSP (https://www.91tcmsp.com/#/database) and PubChem (https://pubchem.ncbi.nlm.nih.gov/) databases. Targets related to psoriasis were gathered from the TTD (https://db.idrblab.net/ttd/), OMIM (https://www.omim.org/), and GeneCards (https://www.genecards.org/) databases. The overlap of targets between the components and psoriasis was visualized using a Venn diagram. A network was then constructed by Cytoscape software (version 3.2.1) [31] linking the targets of components (OB ≥ 30% and DL ≥ 0.18) to psoriasis targets, from which the betweenness centrality and degree values of potentially active ingredients were derived.

2.7. Patient samples

All blood samples from normal people and psoriasis patients were from the Second Affiliated Hospital of Nanjing Medical University and approved by the Ethics Committee of the Second Affiliated Hospital of Nanjing Medical University (No. [2023]-KY-010-01). The severity of the patient is graded by the dermatologist. Serum samples were obtained by centrifugation at 4 °C, 3000 $r \cdot min^{-1}$ for 3 min, and PBMCs were obtained by density gradient centrifugation using Lymphoprep™ reagent (Serumwerk, Germany). Serum levels of IL-6, IFN-β, IL-17, and IL-23 were detected using the human IL-6, IFN-β, IL-17, and IL-23 enzyme-linked immunosorbent assay (ELISA) kits (Biolegend, 430504; 4A Biotech, CHE0274; ZCi BiO, ZC-32412; ZCi BiO, ZC-32426). All studies were carried out following the principles of the Declaration of Helsinki.

2.8. Western blotting

Proteins were extracted using lysis buffer (Beyotime, Wuhan, China, P0013B). Proteins were separated by SDS-PAGE and transferred to PVDF membranes (Millipore, Darmstadt, Germany, IPVH00010POPE). Membranes were blocked with 5% non-fat milk in TBST, then incubated with primary antibodies overnight at 4 °C. After washing, membranes were incubated with HRP-conjugated secondary antibodies for 2 h at room temperature. Signals were detected using an ECL kit (Abbkine, Nanjing, China, BMU102-CN) and imaged with a Bio-Rad imaging system (ChemiDocTMXRS, Bio-Rad, Hercules, USA). The primary antibodies were as follows: β-actin (1∶50 000, Proteintech, Wuhan, China, 66009-1-IG), STING (1∶20 000), p-STING (1∶1000, CST, USA, 50907S), Interferon regulatory factor 3 (1∶1000, IRF3, CST, USA, 4302S), p-IRF3 (1∶1000, CST, USA, 29047S), p-TBK1 (1∶2000, Affinity, OH, USA, AF8190), TBK1 (1∶1000, Abcam, Cambridge, UK, ab40676), NF-κB p65 (1∶200, Santa Cruz, USA, sc-8008), p-NF-κB p65 (1∶1000, CST, USA, 3033S), loricrin (1∶500, ABclonal, Wuhan, China, A21039), and Filaggrin (1∶2000, ABclonal, Wuhan, China, A20011). The secondary antibodies are goat anti-rabbit IgG (H + L) HRP (1∶50 000, Bioworld, Missouda, USA, BS13278) and goat anti-mouse IgG (H + L) HRP (1∶50 000, Bioworld, Missouda, USA, BS12478). ImageJ software was applied to analyze the protein expression levels.

2.9. Immunohistochemistry

Briefly, sections were deparaffinized, subjected to antigen retrieval, and treated with 3% H_2O_2 to block endogenous peroxidase. After blocking with BSA, sections were incubated with primary antibodies targeting IL-6 (1∶400, Affinity, OH, USA, DF6087), IFN-β (1∶100, Affinity, OH, USA, DF6471), TNF receptor-associated factor 6 (TRAF6, 1∶50, Abcam, Cambridge, UK, AB40675), serine/threonine kinase 11 (LKB1, STK11, 1∶200, ABclonal, Wuhan, China, A2122), AMP-activated protein kinase (AMPK, 1∶250, ABclonal, Wuhan, China, A1229), and Unc51-like kinase 1 (ULK1, 1∶200, Proteintech, Wuhan, China, 68445-1-IG), followed by an HRP-conjugated secondary antibody and visualized using DAB (1∶50, Servicebio, Wuhan, China, G1212). The stained sections were imaged with a Mantra Pathology Workstation and analyzed using ImageJ software. The samples were coded by an independent researcher. Subsequent image acquisition, analysis, and scoring were performed by investigators who

were blinded to the group assignments.

2.10. UHPLC-Q-TOF-MS/MS analysis

YXKL, kaempferol, and quercetin were ultrasonically dissolved in methanol. The concentration of YXKL was 0.1 g·mL^{-1}, while the concentrations of quercetin and kaempferol solutions were 4, 7, 15, 31, 62, 125, 250, 500, 1000, and 2000 ng·mL^{-1}, respectively. The solutions were analyzed using an AB SCIEX Triple TOF™ 5600 system (AB Sciex, USA). The samples were injected into a Thermo Acclaim™ RSLC 120 C_{18} column (3.0 mm × 100 mm, 2.2 μm) at 40 °C. The mobile phase consisted of 0.1% formic acid in water (A) and acetonitrile (B) at a flow rate of 0.4 mL·min^{-1}. The gradient elution program was: 0–3 min, 10% B; 3–28 min, 10%–55% B; 28–32 min, 55%–90% B; 32–35 min, 90% B; 35–38 min, 90%–10% B; 38–40.1 min, 10% B. Mass spectrometry was performed using electrospray ionization (ESI) source with the following conditions: ion source temperature, 550 °C; curtain gas, 40 psi; nebulizer gas, 55 psi; auxiliary gas, 55 psi; ion spray voltage, ±5500 V; collision energy, ±40 V; declustering potential, ±100 V. The mass range was scanned from *m/z* 50 to 1500. Data were processed using PeakView Software™ (AB Sciex, USA), and chromatograms were plotted using Origin Pro 9.0 (OriginLab, USA).

2.11. Chemical structural similarity

The structures of compounds were acquired from the PubChem database, and the structure of STING protein (PBD ID: 6MXE) was obtained from the RCSB PBD database (https://www.rcsb.org/). The components in YXKL were compared for structural similarity to the STING inhibitors H-151 and compound 18 using SYBYL-X software (Tripos, USA), and the DoGSiteScorer (https://proteins.plus/) was utilized to predict the potential binding pockets for the components to the STING proteins.

2.12. Drug affinity responsive target stability (DARTS) assay

THP-1 cell lysates were prepared using M-PER Mammalian Protein Extraction Reagent (Thermo, USA, 78503). After centrifugation at 18 000 *g* for 20 min at 4 °C, the supernatant was divided equally into several portions. Each portion was treated with or without a 10 μmol·L^{-1} compound (quercetin or kaempferol) at room temperature for 30 min. Subsequently, pronase (Roche, 10165921001, Basel, Switzerland) was added to each portion at varying concentrations and incubated at room temperature for an additional 30 min. The reaction was terminated by adding 0.5 mol·L^{-1} ethylene diamine tetraacetic acid (EDTA, Macklin, Shanghai, China) and incubating on ice for 15 min. After adding the loading buffer, the samples were heated at 70 °C for 10 min for the Western blotting.

2.13. Cellular thermal shift assay (CETSA)

Lysates from THP-1 cells were centrifuged at 20 000 *g* for 20 min at 4 °C to obtain the supernatant, which was then divided into equal aliquots. After being treated with PBS, 10 μmol·L^{-1} quercetin, or 10 μmol·L^{-1} kaempferol for 30 min at room temperature, the supernatant was divided into 11 equal portions and heated at temperatures ranging from 42 to 62 °C (in 2 °C increments) for 3 min each. After cooling at room temperature for 3 min, the samples were centrifuged again at 20 000 *g* for 20 min at 4 °C to obtain new supernatants, which were used to detect STING protein levels by Western blotting.

2.14. Microscale thermophoresis (MST)

Briefly, the SUMO-His-Tagged STING protein (1.926 nmol·L^{-1}, TargetMol, Shanghai, China, TMPJ-01206) was labeled using RED-tris-NTA His Tag 2nd Generation Dye (100 nmol·L^{-1}, Nano Temper, Munich, Germany, NT-L118). The labeled protein was subsequently mixed with quercetin or kaempferol (the maximum concentration is 0.25 mmol·L^{-1} and then diluted using PBST). The mixtures were then loaded into the capillaries, and MST analysis was performed using the Monolith NT.115 MST instrument (NanoTemper, Munich, Germany).

2.15. Zebrafish model of angiogenesis

Female and male Fli1∶egfp transgenic zebrafish were purchased from Nanjing Yishuhua Biotechnology Co. (Nanjing, China). For zebrafish embryos at 24 h post-fertilization, dechorionation was performed using 0.1 mg·mL^{-1} trypsin, followed by random grouping. After stimulation or no stimulation for 24 h, the juveniles were observed and imaged for neovascularization using a fluorescence microscope (Leica, M205FA, USA). The area of the subintestinal vein (SIV) in zebrafish was quantified using CS6 software (Adobe, USA).

2.16. Tube formation assay

2 × 10^4 HUVECs were seeded per well in a 96-well plate that had been pre-coated with Matrigel (Corning, USA, 354234). Cells were cultured in a cell incubator at 37 °C with 5% CO_2 to observe tube formation. Images were captured using a Zeiss microscope (Zeiss Axio vert A1, Oberkochen, Germany). The number of junctions, number of branches, and branch length of tubules formed by HUVECs were analyzed by ImageJ software.

2.17. Measurement of endothelial monolayer transepithelial electrical resistance (TEER) and permeability

HUVECs were resuspended in a drug-containing or drug-free culture medium and seeded at a density of 2 × 10^5 cells per well in the upper chamber of Transwell inserts (0.4 μm, NEST, Shanghai, China, 724101). The cells were cultured for 24 h to form a monolayer. The integrity of the HUVEC monolayer was assessed by measuring TEER value using a cell impedance meter (Millicell ERS-2, Merck, Germany). 0.1 mg·mL^{-1} FITC-dextran (40 kDa, Sigma, USA) was added to the upper chamber. Every 15 min, 100 μL of the medium from the bottom chamber was collected, and the upper chamber medium was replenished to maintain a constant volume. This process was continued for 1 h. The collected medium was analyzed using a PerkinElmer Victor V fluorescence plate reader (excitation: 480 nm, emission: 520 nm) to quantify the permeability of the HUVEC monolayer.

2.18. Cell adhesion assay

HUVECs were seeded in a 96-well plate and cultured for 24 h to form a monolayer. Calcein AM (Beyotime, Wuhan, China, C2012)-labeled THP-1 cells were added and incubated for 30 min. Non-adherent cells were then removed with PBS. Adhesion efficiency was assessed by counting the adherent Calcein AM-labeled cells under a fluorescent microscope and analyzing the images with ImageJ software.

2.19. Data and statistical analysis

Data are expressed as mean ± standard deviation (SD). Before statistical comparison, the normality of data distribution was assessed using the Shapiro-Wilk normality test and the Kolmogorov-Smirnov normality test. One-way analysis of variance (ANOVA) with Dunnett's multiple comparisons test was performed for multiple comparisons, while an unpaired *t*-test was

used for comparison between the two groups. Statistical significance was set at $P < 0.05$.

3. Results

3.1. YXKL treatment delays the progression of IMQ-induced psoriasis

To evaluate the efficacy and persistence of YXKL in the treatment of psoriasis, we established psoriatic murine models using IMQ cream and assessed the treatment effects on days 3, 5, and 7 post-modeling. We observed the progressive development of characteristic lesions including redness, scaling, thickening, desquamation, and crust formation (Fig. 1A). Model mice exhibited significant weight loss alongside increased PASI scores and right ear thickness compared to controls (Figs. 1B–1D). Treatment with YXKL (1.82 and 3.64 g·kg^{-1}) significantly alleviated these psoriatic features, with ear thickness reduction evident by day 2 and PASI score improvement by day 4 (Figs. 1A–1D). These therapeutic effects were maintained throughout the study period (Figs. 1A, 1C and 1D). Although 3-day YXKL treatment didn't significantly reduce epidermal thickness, prolonged administration effectively inhibited pathological changes, including epidermal thickening, hyperkeratosis, Munro microabscess formation, and dermal vasculature hyperplasia and dilatation (Figs. 1E–1H). These findings demonstrate that YXKL can both mitigate and sustain protection against psoriasis progression.

3.2. YXKL treatment reduces the inflammatory cell infiltration and proinflammatory cytokine production to improve skin barrier impairment

Considering the position of immune cells in the psoriasis pathogenesis, we further examined the effects of YXKL on inflammatory cell infiltration. As expected, YXKL (3.64 g·kg^{-1}) significantly reduced infiltration of pro-inflammatory M1 macrophages and Th17 cells while increasing anti-inflammatory M2 macrophages in psoriatic skin (Figs. 2A–2G). Meanwhile, YXKL was able to significantly reverse the elevated levels of *IL-6*, *IFN-β*, *IL-17A*, and *IL-23* genes in the skin lesions of psoriatic mice (Fig. 2H). These immunomodulatory effects were accompanied by the restoration of skin barrier protein loricrin (1.82 g·kg^{-1} YXKL), although filaggrin remained unchanged (Figs. 2I–2K). These results suggested that YXKL might reduce inflammatory cell infiltration and proinflammatory cytokine release in the skin to alleviate skin barrier damage in psoriasis.

3.3. YXKL treatment alleviates psoriatic skin inflammatory damage by suppressing the activation of the STING/NF-κB signaling pathway

To uncover the mechanisms underlying the anti-psoriatic effects of YXKL, we turned to the GEO database, which revealed abnormal expression of *TMEM173* (STING) and its related genes in psoriatic lesions versus normal skin (Fig. 3A). This pattern was also observed in PBMCs from psoriasis patients (Fig. 3B). However, significant differences in the gene expression of *IRF3*, *RELA*, *NFKB2*, *TRAF6*, and *ULK1*, which are related to the activation of the STING pathway, were noted between mild and severe psoriasis lesional skin (Fig. 3A). Similar disparities in *IRF3*, *RELA*, *NFKB1*, *ULK1*, and *STK11* expression were seen in the lesional skin of Asian intermediate plaque psoriasis (Asian intermediate-LS) and Western large plaque psoriasis (Western large-LS) (Fig. 3C). These results suggested that the STING/NF-κB and STING/IRF3 signaling axes might dominate to varying degrees in psoriasis patients with different severities. To confirm our hypothesis, we collected serum and PBMCs from normal persons and patients with mild, moderate, and severe psoriasis. The age distribution of psoriasis patients was similar across groups (30–50 years) (Fig. 3D). Serum levels of STING-related inflammatory cytokine IL-6 and IFN-β in moderate and severe psoriasis patients were significantly higher than those in normal individuals, while IL-17 and IL-23 were only increased in severe cases (Figs. 3E–3H). Moreover, compared to healthy individuals, the elevation of IL-17 and IL-23 in severe psoriasis patients was less pronounced than that of IL-6 and IFN-β, particularly for IL-23 (Figs. 3E–3H). In psoriatic mice, we discovered that *IFN-β* gene expression increased earlier in the development of psoriasis compared to *IL-23*, while the elevation of *IL-6* occurred later than that of *IFN-β* (Fig. 3I). Moreover, both STING/IRF3 and STING/NF-κB pathways were activated in PBMCs of moderate psoriasis, but only the STING/NF-κB pathway was significantly activated in severe cases, with stronger activation than in moderate psoriasis (Figs. 3J and 3K). STING and TBK1 protein levels were significantly higher in severe psoriasis patients (Figs. 3J and 3K). These findings suggest STING could act as a severity-responsive switch in psoriasis, with IRF3-driven IFN-β production being predominant in early-stage disease, dynamically shifting to NF-κB-mediated IL-6 dominance as the disease progresses, while relegating the IL-17/IL-23 axis to a secondary role.

Our mechanistic investigations revealed that 7-day treatment with YXKL significantly suppressed the activation of the STING/NF-κB pathway in skin lesions without affecting the STING/IRF3 pathway (Figs. 4A and 4B). Consistently, YXKL (3.64 g·kg^{-1}) markedly reduced IL-6 protein levels in dorsal skin lesions while leaving IFN-β unchanged (Figs. 4C–4E), despite downregulating both cytokines at the transcriptional level (Fig. 2H). Moreover, YXKL (3.64 g·kg^{-1}) substantially decreased the expression of *IL-17A* and *IL-23* genes in psoriatic skin (Fig. 2H), an effect potentially attributable to its suppression of IL-6 production. To further elucidate STING pathway modulation, we examined upstream regulators, TRAF6, LKB1, AMPK, and ULK1 [32, 33]. Examination of upstream STING regulators showed YXKL (3.64 g·kg^{-1}) only modestly attenuated IMQ-induced TRAF6 upregulation without affecting LKB1, AMPK, or ULK1 (Figs. 4C, 4F–4I). Collectively, our findings indicate that YXKL exerts anti-psoriasis effects primarily by inhibiting the STING/NF-κB pathway, rather than the STING/IRF3 pathway, which may consequently reduce inflammatory cell infiltration and proinflammatory cytokine release, thereby alleviating skin barrier damage in psoriasis.

3.4. Discovery of quercetin and kaempferol, the flavonoid components in YXKL, as potential STING inhibitors

To identify the active components in YXKL that exert an anti-psoriasis effect by targeting STING, we first employed UHPLC-Q-TOF-MS/MS and detected 29 compounds (Fig. 5A, Table S2). We then used TCMSP and PubChem databases to gather information and targets for these compounds and combined this with psoriasis-related targets from the TTD, OMIM, and GeneCards databases. By mapping the network and analyzing parameters such as the number of co-targets, oral bioavailability (OB), drug-likeness (DL), and degree, we identified quercetin, kaempferol, eriodictyol, pratensein, taxifolin, and morin as potential active ingredients in YXKL for psoriasis treatment (Table S3). By comparing the structural similarity of these compounds to known STING inhibitors, such as H-151 and compound **18**, we found that among the six identified components, kaempferol and quercetin exhibited the highest structural similarity to these STING inhibitors (Table S4). Furthermore, the potential binding pocket predicted by DoGSiteScorer showed high similarity to the STING binding pocket reported for compound **18** [34], with both kaempferol and quercetin well-docked into this active site (Fig. 5B, Table S5). Critically,

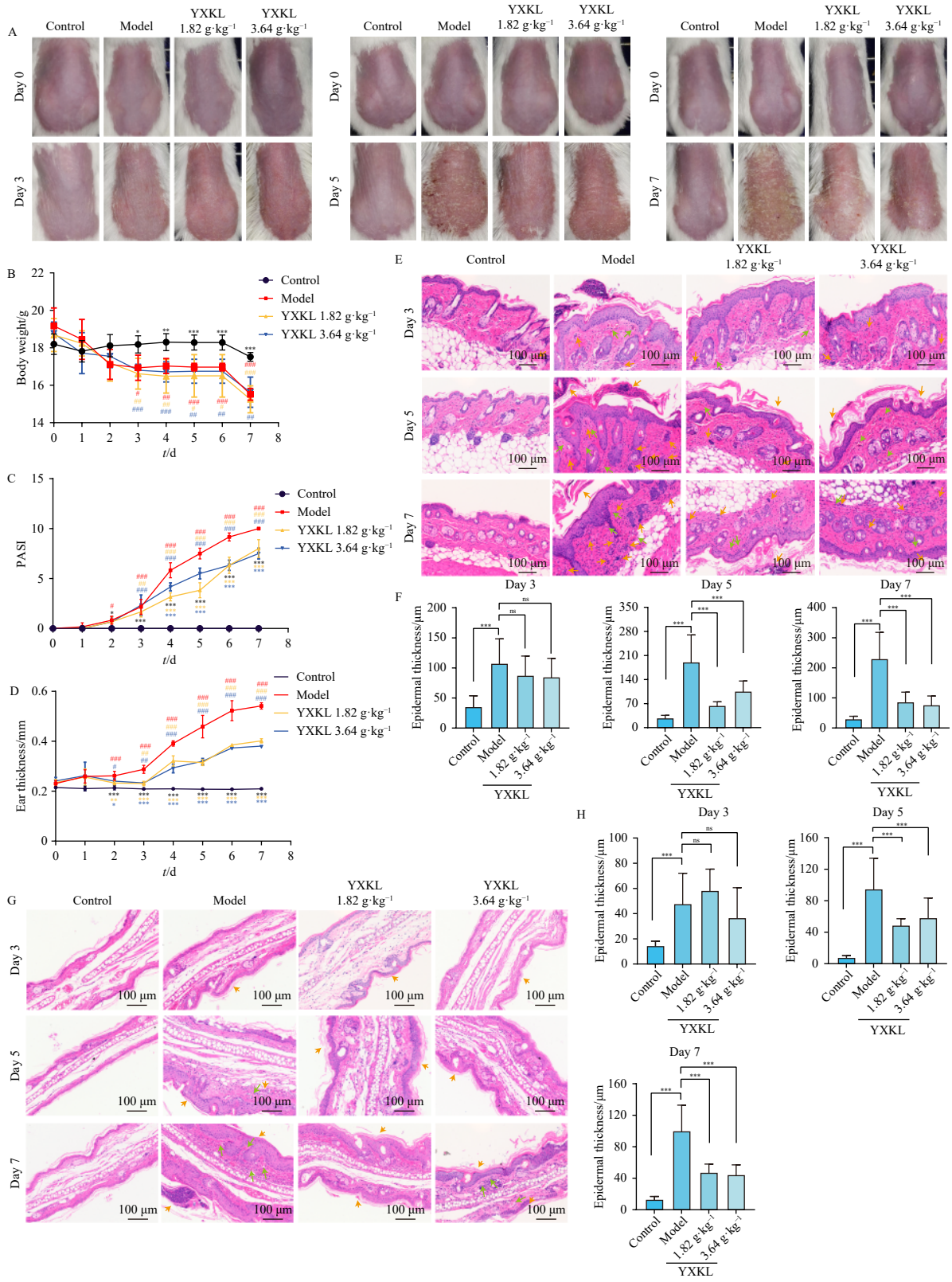
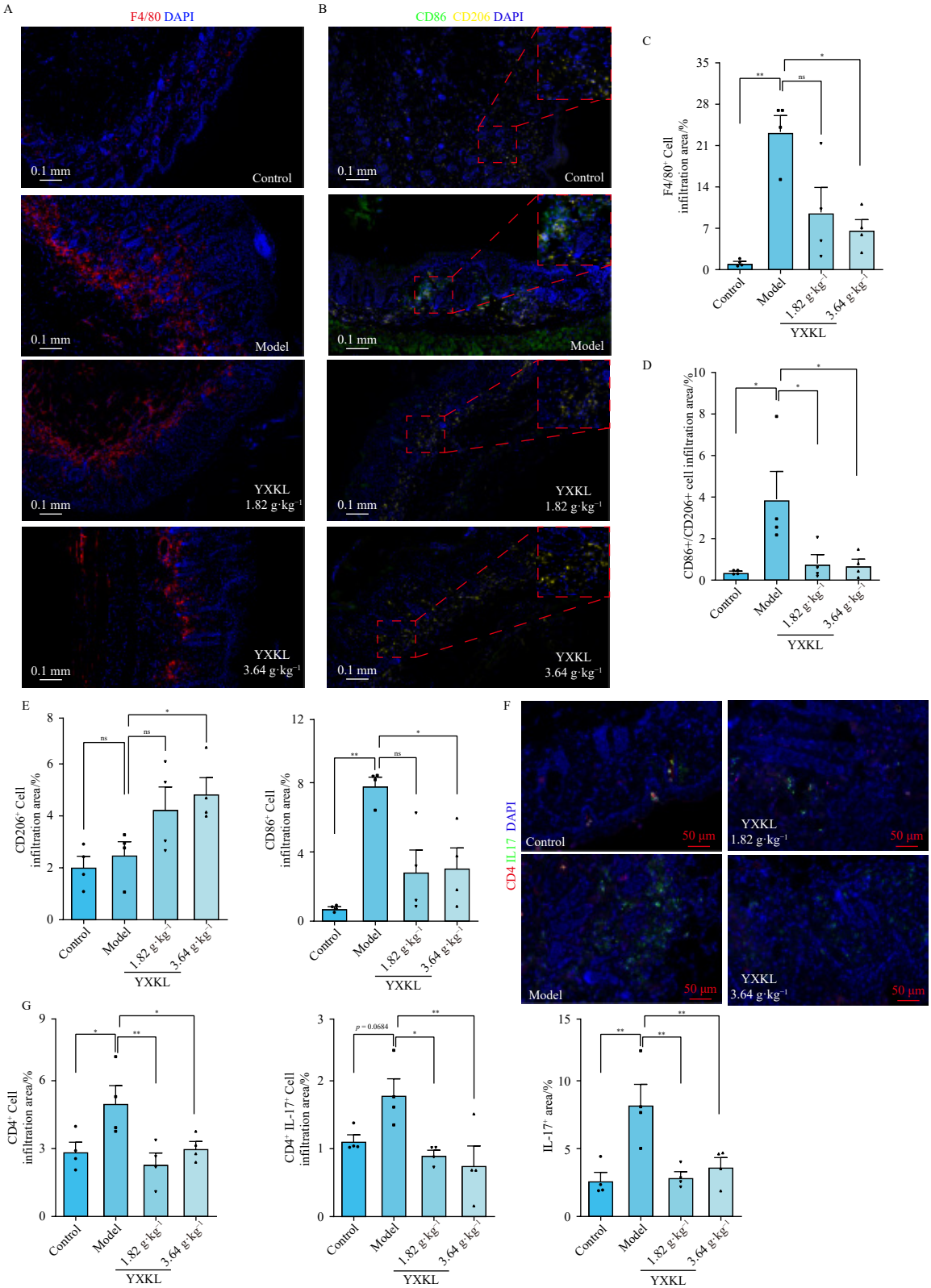


Fig. 1 YXKL treatment alleviates IMQ-induced psoriatic lesions. (A) Appearance of murine skin (n = 6). (B) Body weight (n = 6). (C) The PASI score (n = 6). (D) Ear thickness (n = 6). (E) HE staining of dorsal mouse skin on days 3, 5, and 7 after initiation of modeling and treatment (n = 3). (F) The epidermal thickness of dorsal skin (n = 3). (G) HE staining of mouse ear skin on days 3, 5, and 7 after initiation of modeling and treatment (n = 3). (H) The epidermal thickness of ear skin (n = 3). Green arrows highlight vasculature hyperplasia and dilatation, whereas orange arrows indicate infiltrating immune cells, hyperplastic epidermis, and Munro microabscesse. Data are expressed as mean ± SD, $^{*}P < 0.05$, $^{**}P < 0.01$, $^{***}P < 0.001$ *vs* model group. $^{\#}P < 0.05$, $^{\#\#}P < 0.01$, $^{\#\#\#}P < 0.001$ *vs* control group.

HPLC-MS quantification confirmed that these two top-ranked flavonoids were also major constituents of the formula, with concentrations reaching 1053.97 and 1245.64 ng·mL^{-1}, respectively, in a 0.1 g·mL^{-1} YXKL solution (Fig. S1A, Table S6). At 10 μmol·L^{-1}, they exhibited notable anti-inflammatory effects by effectively reducing the LPS-induced mRNA levels of *IL-6*, *IL-23*, *IFN-β*, and *TNF-α* (Figs. S1B–S1E). Kaempferol additionally reversed the LPS-induced elevation of *IL-1β* (Fig. S1F), suggesting that they might

exert an anti-psoriasis dermatitis by targeting STING. To validate the STING-binding capability of kaempferol and quercetin, we performed combined DARTS and CETSA analyses, which confirmed their binding to STING proteins at 10 μmol·L^{-1} (Figs. 5C–5F). However, MST revealed moderate binding affinities (K_d = 99.306 ± 0.131 μmol·L^{-1} for quercetin and 60.158 ± 0.069 μmol·L^{-1} for kaempferol), likely limited by the compounds' solubility (Fig. S1G). We believe solubility limitations may underestimate the true binding potential of these compounds, as the binding at functional concentrations demonstrates their potential as the sting regulatory component in YXKL. Further experiments studying their influence on the STING signaling pathway showed that neither kaempferol nor quercetin affected STING gene expression in THP-1 cells, but both significantly inhibited the elevation of *IFN-β* induced by the STING endogenous ligand cGAMP (Fig. 5G, S1H). At 10 μmol·L^{-1}, quercetin and kaempferol effectively attenuated cGAMP-triggered activation of the STING/NF-κB and STING/IRF3 pathways (Figs. 5H and 5I). These results



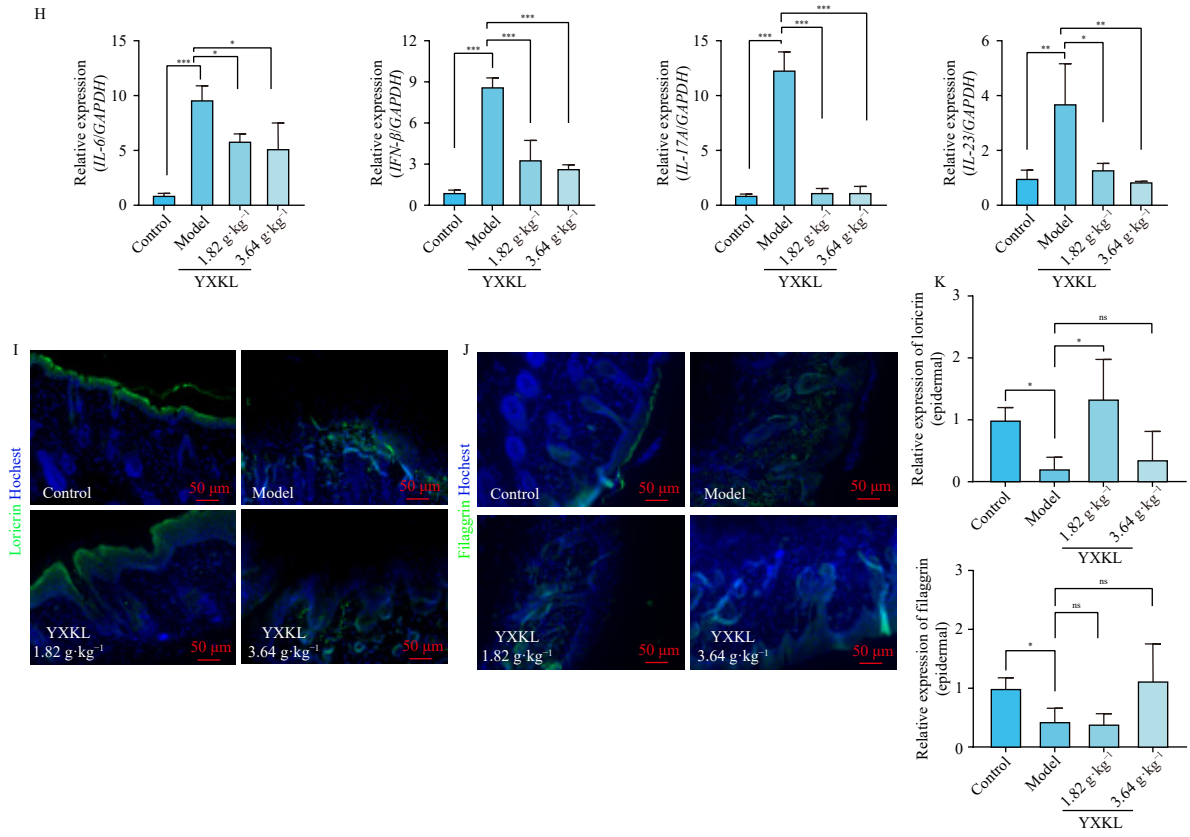


Fig. 2 YXKL treatment reduces the inflammatory cell infiltration and proinflammatory cytokine production to improve skin barrier impairment after 7 d of treatment with IMQ cream and YXKL, immunofluorescence analysis was performed on the dorsal skin lesions of mice. (A) Representative image of F4/80$^+$ cell infiltration areas (n = 4). (B) Representative staining of CD86$^+$ cell infiltration and CD206$^+$ cell infiltration areas (n = 4). (C) Quantification of the F4/80$^+$ cell infiltration areas (n = 4). (D) The ratio of CD86$^+$ and CD206$^+$ cell infiltration area (n = 4). (E) Quantification of the CD206$^+$ and CD8$^+$ cell infiltration area after 7 d of treatment with IMQ cream and YXKL (n = 4). (F) Representative staining of CD4$^+$ IL17$^+$ T cell infiltration areas. (G) Quantification analysis of CD4$^+$ T cell infiltration, CD4$^+$IL17$^+$ T cell infiltration, and IL-17$^+$ areas (n = 4). (H) mRNA levels of *IL-6, IFN-β, IL-17A,* and *IL-23* in back skin lesions after 7 d of IMQ and YXKL treatment (n = 3). (I–K) Representative staining and quantification analysis of the epidermal skin barrier-related proteins loricrin and filaggrin (n = 3). Data are expressed as mean ± SD, $^*P < 0.05$, $^{**}P < 0.01$, $^{***}P < 0.001$.

collectively identified quercetin and kaempferol as STING-targeting flavonoid components of YXKL, which bind to the STING protein and inhibit the activation of the STING signaling pathway.

3.5. Quercetin and kaempferol alleviate psoriatic keratinocyte inflammation via STING pathway inhibition

Considering the pivotal role of keratinocytes in psoriatic inflammation, we then investigated the effects of quercetin and kaempferol from YXKL using two distinct stimulation models that mimic different disease severity levels: IMQ (moderate) and M5 (severe). In IMQ-stimulated HaCaT cells, neither compound altered loricrin or filaggrin expression (Fig. S2A). By contrast, under M5 stimulation, which incorporates multiple psoriasis-relevant cytokines, kaempferol significantly increased loricrin expression while quercetin showed a modest elevation (Fig. S2A). Both compounds differentially modulated inflammatory mediators of the two models as demonstrated by their effects in IMQ-induced HaCaT cells, where 10 μmol·L^{-1} treatments downregulated *IL-1β* and *CCL20* mRNA without affecting *IL-6*, *IFN-β*, or *CCL2* (Figs. 6A, S2B). In the M5 model, quercetin markedly suppressed the gene expression of *IL-6*, *IL-1β*, *CCL2*, and *CCL20*, whereas kaempferol significantly reduced *IL-6* and *IL-1β* (Figs. 6B, S2C), with *CXCL10* remaining unchanged in both models (Figs. S2B and S2C). When evaluated in PBMCs representing systemic immunity, only kaempferol inhibited M5-induced *IL-1β* upregulation (Fig. S2D), suggesting that kaempferol and quercetin preferentially target epidermal inflammation. Mechanistic investigations revealed that both compounds (10 μmol·L^{-1}) suppressed STING/NF-κB activation in IMQ/M5-treated HaCaT cells (Figs. 6C, S2E), with quercetin reducing IMQ-induced IRF3 phosphorylation and kaempferol showing similar effects in M5-treated cells (Figs. 6C, S2E). The STING-dependence was further validated through cGAMP reversal experiments, which abolished their inhibition of *IL-6*, *IL-1β*, and *CCL2* (Figs. 6D, S2F). Moreover, the inhibitory effects of YXKL-containing serum (YXKL-SD) on the elevated gene expression of *IL-6* and *CCL20* in M5-induced HaCaT cells were also reversed by the addition of cGAMP (Fig. S2G). These data implied that kaempferol and quercetin in YXKL ameliorate psoriatic keratinocyte inflammation through STING pathway suppression while differentially enhancing loricrin expression.

3.6. YXKL targets STING-high expressed endothelial cells to ameliorate psoriatic vascular dysfunction by inhibiting angiogenesis and restoring vascular integrity

Beyond epidermal effects, we asked whether YXKL could improve psoriatic vascular abnormalities, given the role of STING in angiogenesis. In IMQ-induced psoriatic murine, we observed increased subcutaneous blood vessel length, branching, and branch length (Figs. 7A and 7B). YXKL treatment significantly attenuated these pathological changes, reducing the vessel length, branch number, and branch length in the psoriatic dorsal skin (Figs. 7A and 7B). Immunofluorescence analysis revealed that 3.64 g·kg^{-1} YXKL decreased neovessel formation (CD31-positive areas), and enhanced vascular stabilization through increased endothelial junction protein ZO-1 expression (CD31$^+$ ZO-1$^+$ areas) (Figs. 7C–7F). Although VE-cadherin expression remained unchanged, the α-SMA coverage of blood vessels significantly increased after 1.82 g·kg^{-1} YXKL treatment (Figs. 7G–7J), indicating improved vessel maturation. Importantly, we found that ECs in psoriatic skin exhibited higher STING gene expression (Fig. 7K). STING

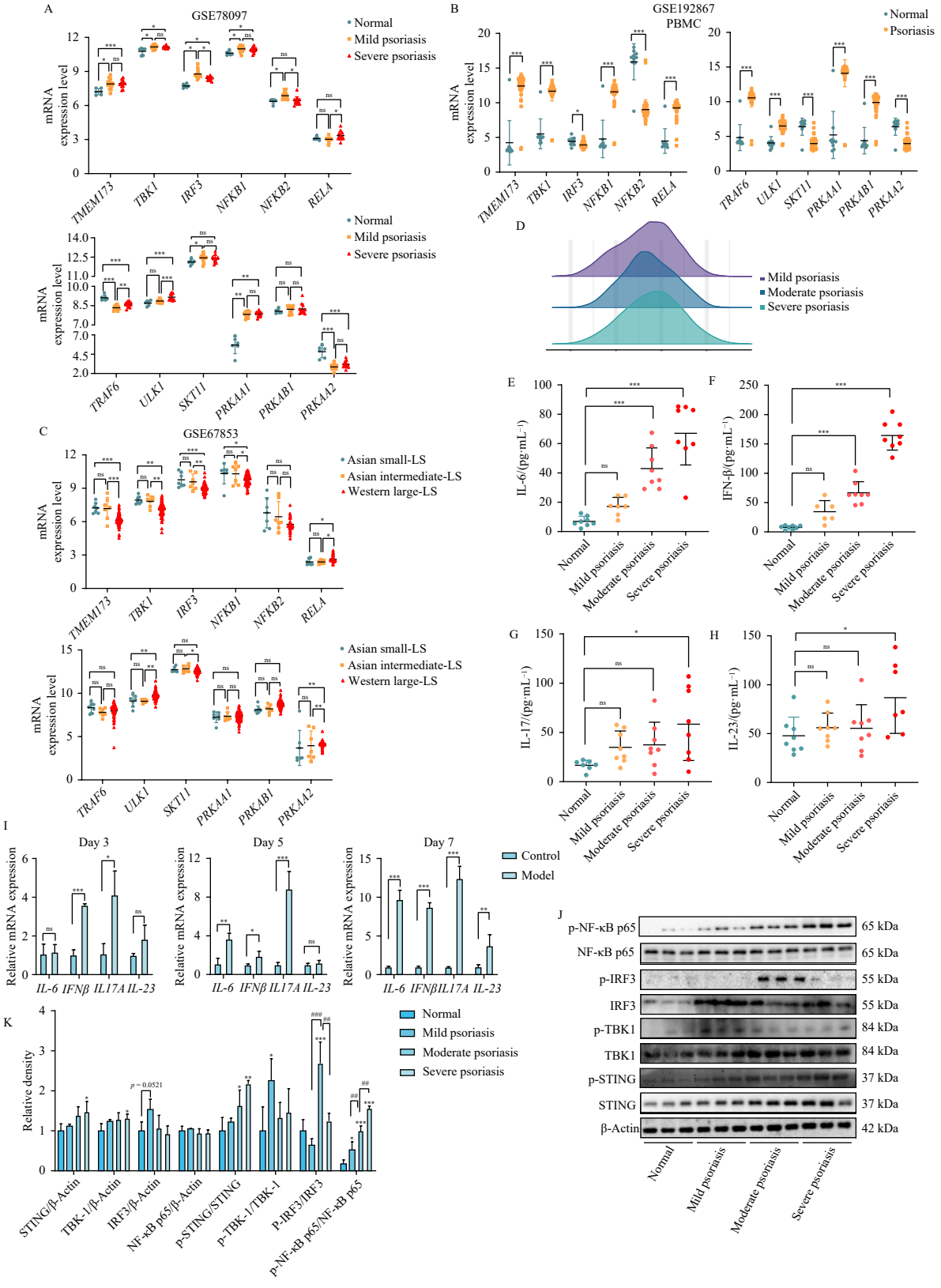


Fig. 3 Dynamic interplay of STING/IRF3 and STING/NF-κB signaling in psoriasis pathogenesis. (A) Analysis of gene expression of *TMEM173*, *TBK1*, *IRF3*, *NFKB1*, *NFKB2*, *RELA*, *TRAF6*, *ULK1*, *STK11*, *PRKAA1*, *PRKAB1*, and *PRKAA2* in normal, mild, and severe psoriasis lesional skin (6 normal, 14 mild, and 13 severe samples). The values were acquired from the GEO database. Accession number: GSE78097. (B) Expression analysis of *TMEM173*, *TBK1*, *IRF3*, *NFKB1*, *NFKB2*, *RELA*, *TRAF6*, *ULK1*, *STK11*, *PRKAA1*, *PRKAB1*, and *PRKAA2* genes in the normal (n = 10) and psoriatic (n = 62) PBMCs. The values were acquired from the GEO database. Accession numbers: GSE192867. (C)Analysis of gene expression of *TMEM173*, *TBK1*, *IRF3*, *NFKB1*, *NFKB2*, *RELA*, *TRAF6*, *ULK1*, *STK11*, *PRKAA1*, *PRKAB1*, and *PRKAA2* in the lesional skin of Asian small plaque psoriasis (Asian small-LS, n = 7), Asian intermediate plaque psoriasis (Asian intermediate-LS, n = 7) and Western large plaque psoriasis (Western large-LS, n = 130). The values were acquired from the GEO database. Accession numbers: GSE67853. (D) Age distribution of collected psoriasis patients (n = 8). (E–H) Serum levels of IL-6, IFN-β, IL-17, and IL-23 in normal people and patients with mild, moderate, and severe psoriasis (n = 8). (I) IMQ cream was applied to construct psoriatic mice. The mRNA levels of *IL-6*, *IFN-β*, *IL-17A*, and *IL-23* in murine back skin lesions after 3, 5, and 7 d of IMQ treatment (n = 3). (J and K) The protein expression of STING, p-STING, TBK1, p-TBK1, IRF3, p-IRF3, NF-κB p65, and p-NF-κB p65 in the PBMC from normal people and patients with mild, moderate, and severe psoriasis. The quantification analysis is shown in (K) (n = 3). Data are expressed as mean ± SD, $^{*}P < 0.05$, $^{**}P < 0.01$, $^{***}P < 0.001$ *vs* Normal; $^{\#}P < 0.05$, $^{\#\#}P < 0.01$, $^{\#\#\#}P < 0.001$ *vs* moderate psoriasis.

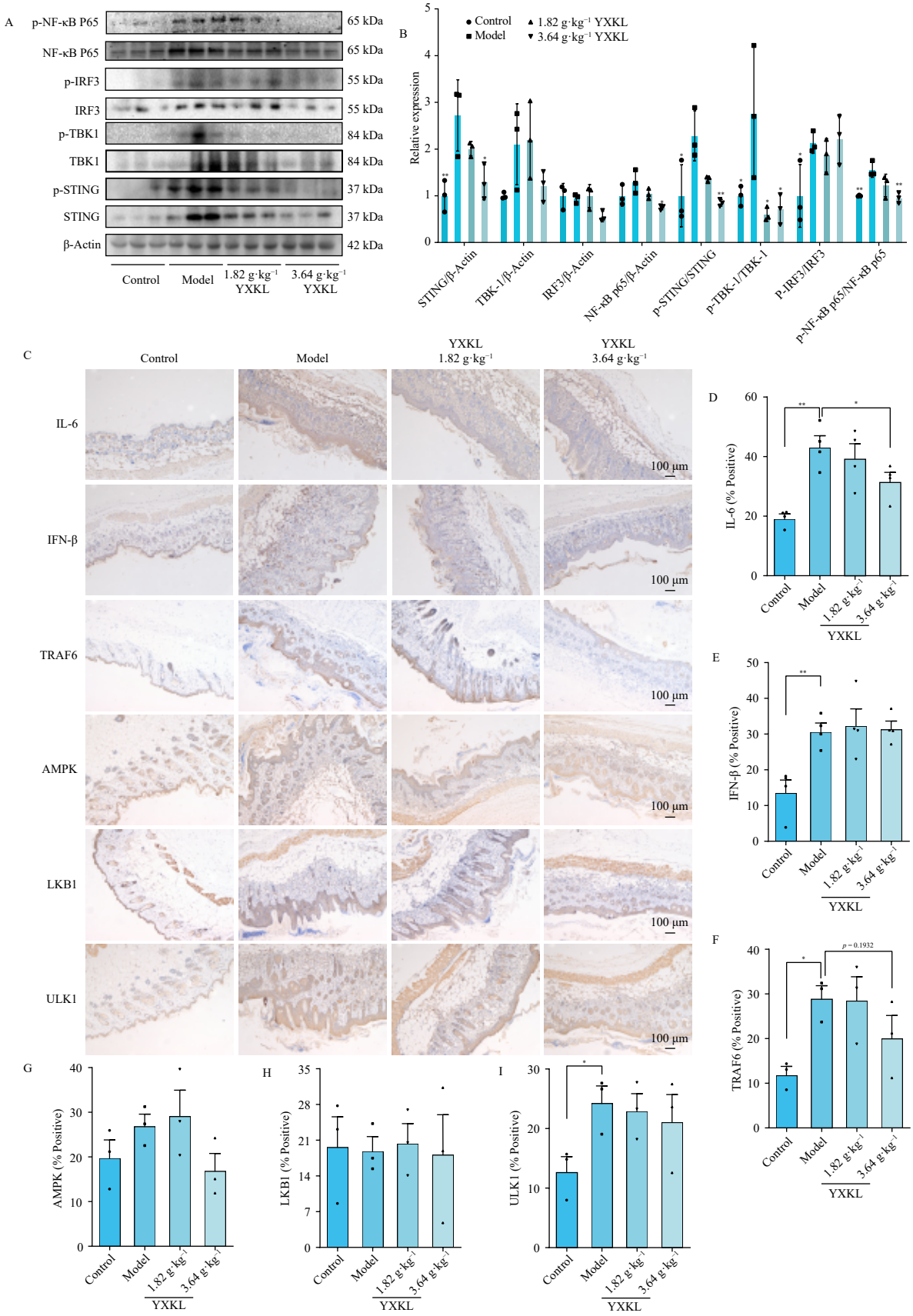


Fig. 4 YXKL mitigates psoriasis by suppressing the activation of the STING/NF-κB signaling pathway after 7 days of treatment with IMQ cream and YXKL, Western blot analysis and immunohistochemistry were performed on the dorsal skin lesions of mice. (A) The protein expression of STING, p-STING, TBK1, p-TBK1, IRF3, p-IRF3, NF-κB p65, and p-NF-κB p65. The quantification analysis is shown in (B) (n = 3). (C) Representative images of immunohistochemistry for IL-6, IFN-β, TRAF6, AMPK, LKB1, and ULK1. Quantitative analysis of the positive percentage in each group is shown in (D–I) (IL-6, IFN-β, n = 4; TRAF6, AMPK, LKB1, and ULK1, n = 3). Data are expressed as mean ± SD, $^{*}P < 0.05$, $^{**}P < 0.01$, $^{***}P < 0.001$.

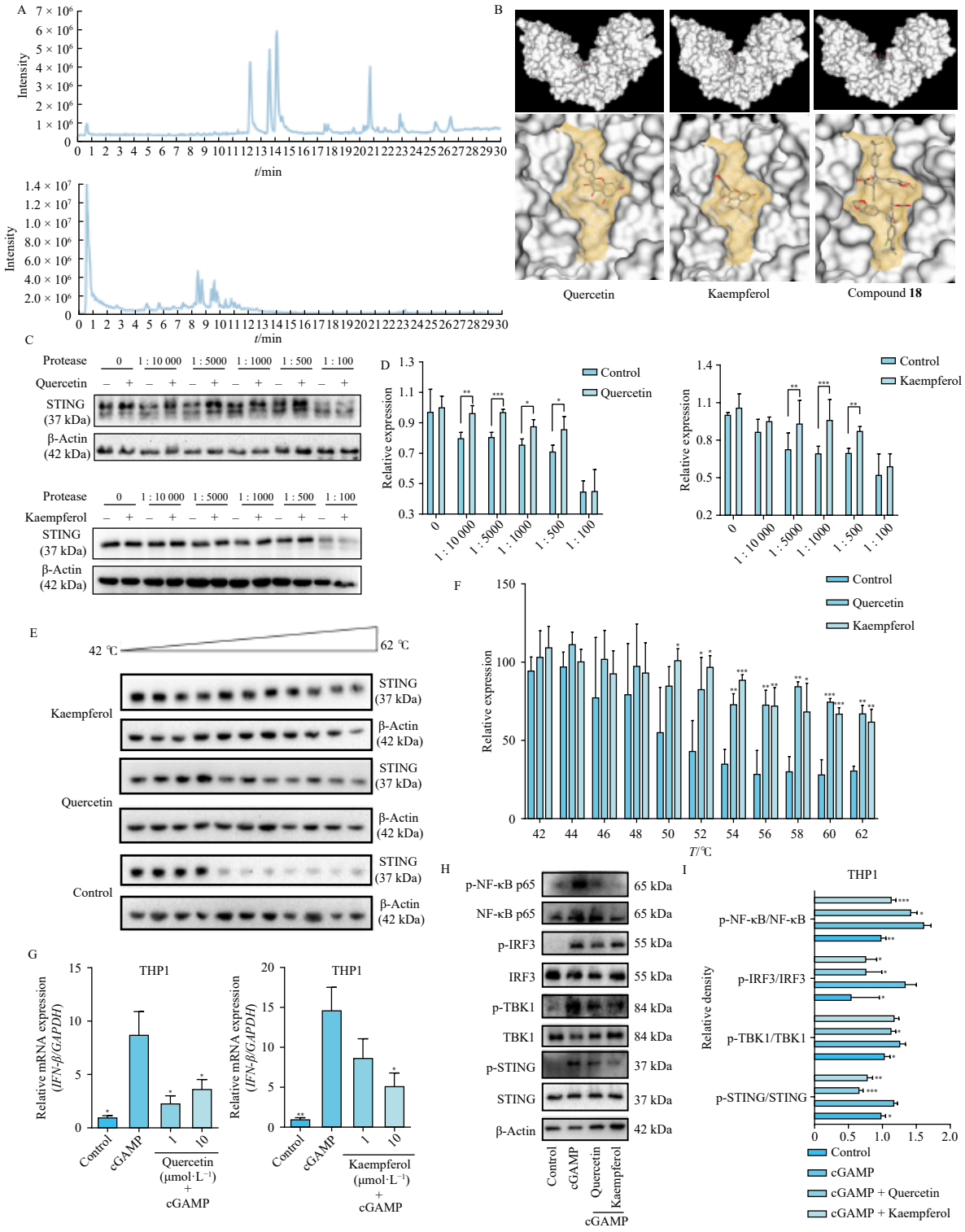


Fig. 5 Quercetin and kaempferol are potential STING inhibitors from YXKL. (A) Base peak ion current chromatograms of YXKL detected by UHPLC-Q-TOF-MS/MS in positive (upper) and negative (lower) ion modes. (B) The predicted binding pocket of quercetin, kaempferol, and compound 18 to STING protein using DoGSiteScorer. (C–F) The binding of 10 μmol·L^{-1} quercetin and kaempferol with STING was detected by DARTS assay and CETSA assay. (D, F) Quantification analysis of the relative STING expression (n = 3). (G) Effect of quercetin and kaempferol on mRNA levels of *IFN-β* in cGAMP-stimulated THP-1 cells (n = 3). (H) Effect of quercetin and kaempferol on the protein expression of STING, p-STING, TBK1, p-TBK1, IRF3, p-IRF3, NF-κB p65 and p-NF-κB p65 in cGAMP-stimulated THP-1 cells (n = 3). (I) Quantification analysis of the expression of p-STING/STING, p-TBK1/TBK1, p-IRF3/IRF3, and p-NF-κB p65/NF-κB p65 (n = 3). Data are expressed as mean ± SD, $^{*}P < 0.05$, $^{**}P < 0.01$, $^{***}P < 0.001$ *vs* cGAMP group.

protein levels were notably elevated in HUVECs compared to HaCaT, THP-1, and PBMCs (Figs. 7L and 7M). Furthermore, significant STING expression was observed in ECs within psoriatic murine skin lesions (Fig. 7N). 3.64 g·kg^{-1} YXKL markedly decreased the STING expression in vascular endothelial cells (Figs. 7N and 7O).

Given these observations, we hypothesize that the therapeutic effects of YXKL on blood vessels may be mediated through the inhibition of STING in the endothelial cells. We employed kaempferol and quercetin, the STING-inhibiting components from YXKL, for verification. We found that 10 μmol·L^{-1} quercetin and kaempferol did not affect the viability of HUVECs under M5 stimulation (Fig. 8A). However, both compounds demonstrated potent anti-angiogenic activity, significantly reducing SIV area in zebrafish

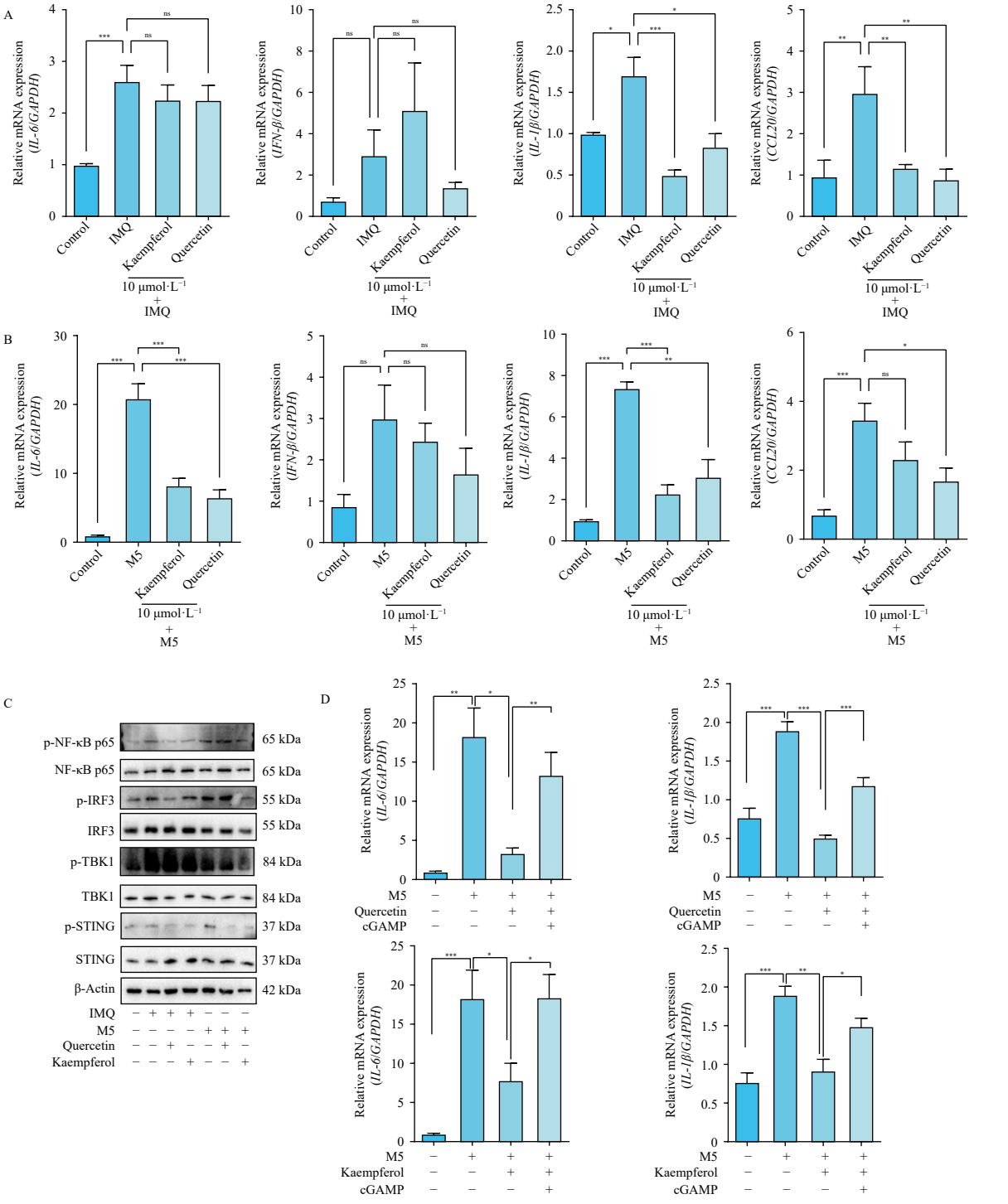


Fig. 6 STING inhibition by quercetin and kaempferol alleviates keratinocyte inflammation *in vitro* psoriatic models HaCaT cells were treated with IMQ or M5 in the presence or absence of quercetin or kaempferol for 24 h. (A and B) The mRNA expression levels of *IL-6*, *IFN-β*, *IL-1β*, and *CCL20* were measured by q-PCR (n = 3). (C) The protein levels of STING, p-STING, TBK1, p-TBK1, IRF3, p-IRF3, NF-κB p65, and p-NF-κB p65 were detected by Western blot assay (n = 3). (D) HaCaT cells were incubated in M5 with or without kaempferol or quercetin for 24 h in the presence or absence of cGAMP. The mRNA expression of *IL-6* and *IL-1β* was measured by q-PCR (n = 3). Data are expressed as mean ± SD, $^{*}P < 0.05$, $^{**}P < 0.01$, $^{***}P < 0.001$.

models and decreasing tube formation capacity (junctions, branches, and branch lengths) in M5-induced HUVECs (Figs. 8B, 8C and S3A). Additionally, they effectively reversed M5-induced endothelial monolayer permeability, restored TEER values, and attenuated the adhesion of THP-1 cells to endothelial cells (Figs. 8D, 8E, S3C and S3D). Mechanistically, although 10 μmol·L^{-1} treatments inhibited the expression of STING protein in M5-stimulated HUVECs without affecting STING activation status, they markedly suppressed phosphorylation of downstream effectors IRF3 and NF-κB p65 (Figs. 8G and S3E). Moreover, the addition of cGAMP abolished the inhibitory effects of kaempferol and quercetin on tube formation and endothelial barrier function (Figs. 8H, 8I, S3F and S3G). Consistent with the results from kaempferol and quercetin, YXKL-SD effectively reversed M5-induced endothelial monolayer permeability and restored TEER values (Figs. S3H and S3I). Crucially, these protective effects were also abolished by the addition of cGAMP (Figs. S3H and S3I). Therefore, the inhibition of angiogenesis and restoration of vascular integrity in psoriatic mice by YXKL were mediated through its flavonoid components kaempferol and quercetin, which down-

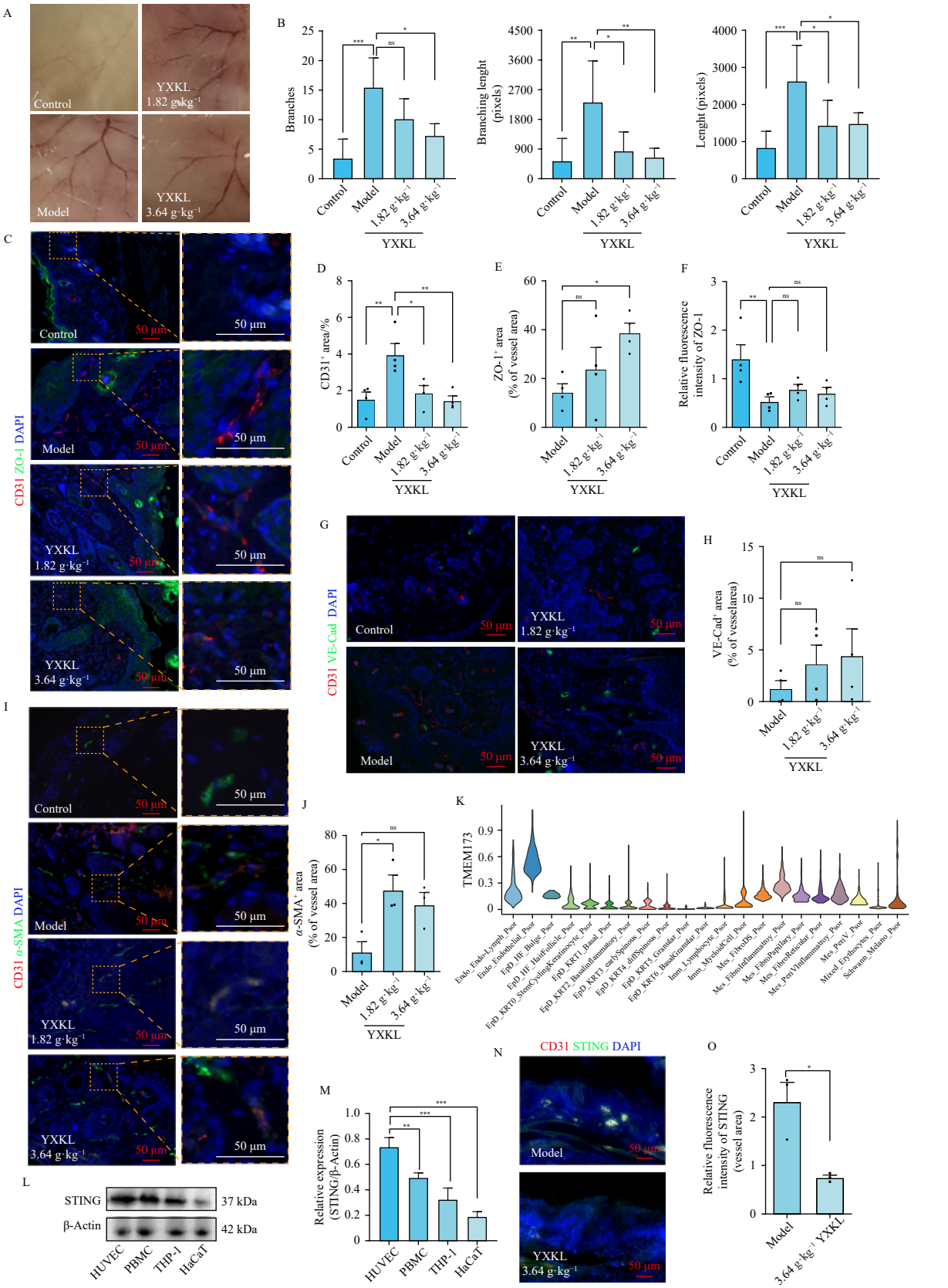


Fig. 7 YXKL ameliorates STING-high-expressing endothelial cell-associated psoriatic vascular dysfunction by suppressing angiogenesis and improving vessel integrity. (A) Photographs of the subcutaneous blood vessels on the backs of mice treated with IMQ cream and YXKL on day 7. Length, branch number, and branch length of subcutaneous blood vessels were shown in (B) (n = 6). (C) Representative images for the co-staining of CD31 with ZO-1 in the dorsal skin lesions (n = 4). (D) The percentage of $CD31^+$ area (n = 4). (E) The percentage of $CD31^+$ $ZO\text{-}1^+$ area (n = 4). (F) The relative fluorescence intensity of ZO-1 (n = 4). (G) Immunofluorescence co-staining of CD31 with VE-Cadherin in dorsal skin lesions of psoriatic mice on day 7 (n = 4). (H) The percentage of $CD31^+$ $VE\text{-}Cadherin^+$ area (n = 3). (I) Representative images for the co-staining of CD31 with α-SMA in the dorsal skin lesions (n = 3). (J) The percentage of $CD31^+$ $\alpha\text{-}SMA^+$ area (n = 3). (K) Gene expression of *STING* in different skin cells of psoriasis patients in the CellAtlasPsoriaticSkin database. (L and M) Protein expression of STING in HUVEC, PBMC, THP-1, and HaCaT cells (n = 3). (N and O) Immunofluorescence co-staining of CD31 and STING in skin lesions of psoriatic mice (n = 3). Data are expressed as mean ± SD, $^*P < 0.05$, $^{**}P < 0.01$, $^{***}P < 0.001$.

regulated endothelial STING expression and suppressed the activation of downstream IRF3 and NF-κB p65.

4. Discussion

Psoriasis is a global skin disease with diverse phenotypes that requires varied treatment strategies. Although anti-TNF biologics effectively reduce skin inflammation and angiogenesis, some psoriasis patients develop psoriasiform symptoms with TNF inhibitors [4-6]. Moreover, not all patients benefit from first-line biologics. Pre-treatment LPS-induced NF-κB phosphorylation in DC cells of patients can predict adalimumab non-response [35]. Although IL-6 levels decline with treatment for psoriasis, IL-6 targeted therapy is often ineffective or harmful for plaque

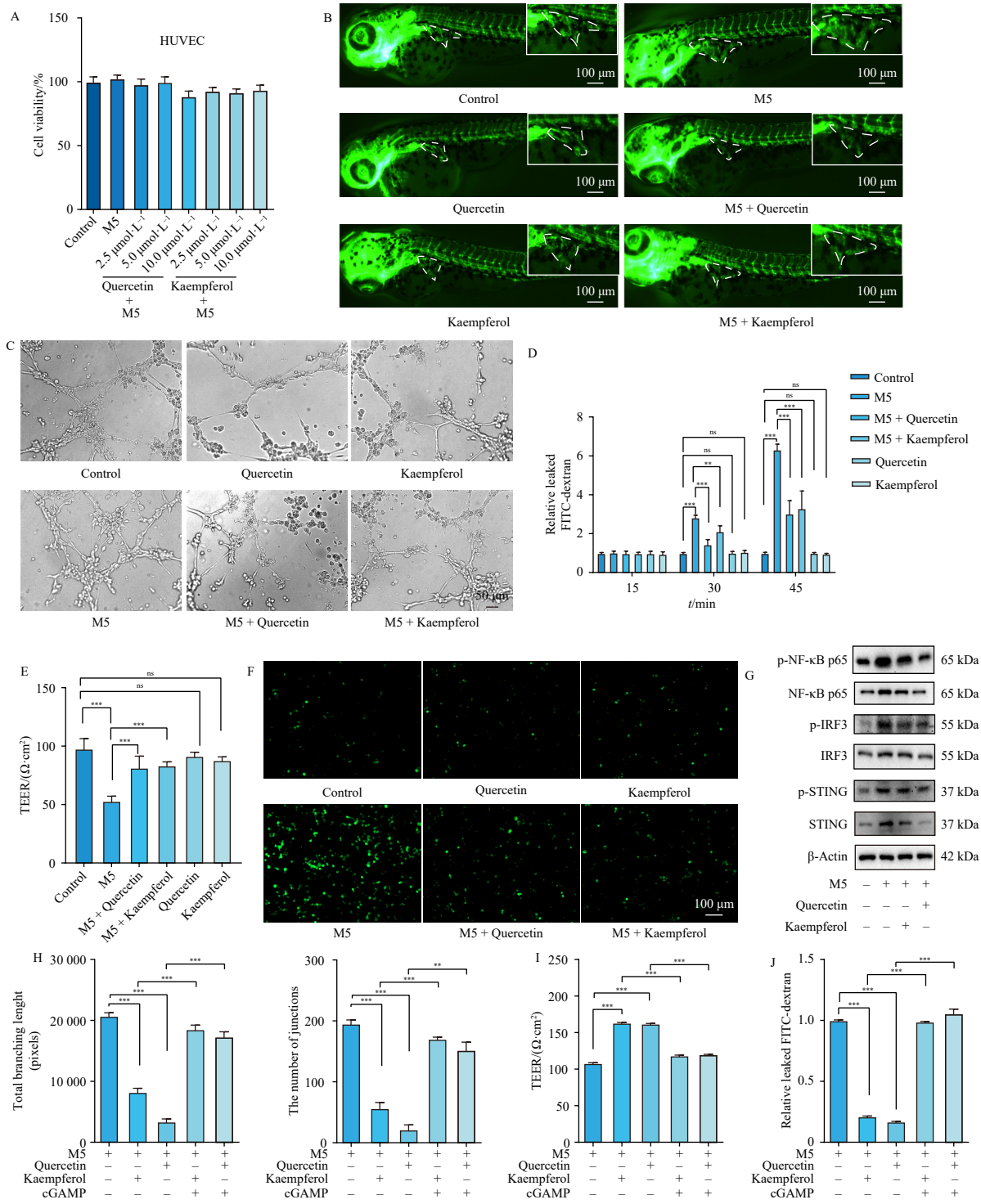


Fig. 8 Quercetin and kaempferol improve psoriatic angiogenesis and vascular integrity *via* endothelial STING downstream signaling suppression. (A) The cell viability of HUVEC treated with and without quercetin or kaempferol under M5 stimulation for 24 h (n = 6). (B) Effects of quercetin and kaempferol on M5-stimulated subintestinal vascularization in zebrafish (n = 5). (C) Representative images of tube formation (n = 3). (D) The permeability of a monolayer of HUVECs was detected using FITC-Dextran (n = 3). (E) The TEER value of monolayer HUVECs was determined by the resistance method (n = 3). (F) Images of calcein AM-labeled THP-1 cell adhering to a monolayer of HUVECs (n = 3). (G) The expression of STING pathway-related proteins in HUVECs treated with quercetin or kaempferol under M5 stimulation. (H–J) Quantitative analysis of the total branching length and number of tube junctions formed by HUVECs treated with quercetin or kaempferol, with or without cGAMP in the presence of M5 stimulation, as well as TEER values, and FITC-Dextran leakage (n = 3). Data are expressed as mean ± SD, $^{**}P < 0.01$, $^{***}P < 0.001$.

psoriasis, but may benefit pustular psoriasis [36, 37]. IL-6 deficiency can also upregulate other proinflammatory cytokines, such as TNF-α [37]. Thus, long-term targeting of a specific cytokine may disrupt cytokine balance and impair immune surveillance. In this context, the multi-component natural formulation YXKL offers a promising alternative. Our experiments demonstrate that YXKL reduces Th17 cell and M1 macrophage infiltration, downregulates key psoriatic cytokines (IL-17, IL-23, IL-6, IFN-β), and reverses pathological angiogenesis. Notably, the multi-component nature of YXKL suggests its therapeutic effects extend beyond STING inhibition, with constituents like taxifolin and morin targeting the JAK-STAT pathway [38, 39], contributing to its broad efficacy. This multi-target and multi-mechanistic action contrasts with the singular focus of most biologics and small-molecule drugs, potentially offering a more comprehensive network regulation, broader efficacy, and a lower risk of therapeutic escape and disease flares. Coupled with its established safety profile from decades of use and inherent cost-effectiveness, YXKL presents a compelling treatment strategy for long-term disease management and accessibility.

In our study, we observed that inflammatory factors exhibit phased dynamics during psoriasis progression, with IFN-β likely triggering the initial inflammatory response, while IL-6 contributes to the amplification and chronicity of inflammation. Although elevated IL-17/IL-23 levels are well-documented in psoriasis, our analysis stratified by disease severity revealed that significant increases in these cytokines occurred only in severe cases. Mouse experiments corroborated this staged cytokine activation, with *IFN-β* preceding *IL-6* and *IL-23*. Further supporting this temporal regulation, we found differential activation of STING/NF-κB versus STING/IRF3 pathways in PBMCs from patients with varying disease severity, suggesting a dynamic interplay between these signaling pathways during disease progression. Given the promoting effect of IL-6 on the Th17 cell differentiation and IL-23 secretion [40, 41], IL-17/IL-23 likely act as late-phase amplifiers, not initiators, of inflammation. This implies that STING-targeted interventions may achieve superior efficacy in early-stage psoriasis by intercepting the pathogenic cascade upstream of Th17 activation. Indeed, YXKL significantly inhibited the activation of the STING/NF-κB pathway, with its therapeutic effects on psoriatic lesions evident by the third day of treatment and sustained throughout the modeling period. Among the 29 components detected in YXKL, kaempferol and quercetin were identified as active ingredients targeting STING, capable of binding to STING proteins and inhibiting cGAMP-induced STING pathway activation.

The inflammatory cascade in psoriasis is driven by complex interactions among immune cells, keratinocytes, and ECs, which collectively impact the efficacy of psoriasis treatments. Spatial transcriptomics shows that successful IL-23 monotherapy reduces IL-17 signaling by decreasing the number of IL-17-producing T cells in lesions and requires a > 90% reduction in IL-17 response in lymphocyte-proximal keratinocytes [42]. However, treatment failure may occur due to excessive IL-23 production, overactive IL-17 signaling, or heightened keratinocyte sensitivity to IL-17 [42]. IL-17-induced reprogramming of the urea cycle increases polyamines in keratinocytes, which activate skin-resident dendritic cells to produce IL-6, enhancing IL-17 secretion and forming a feedback loop that exacerbates psoriasis inflammation [43]. The inflammatory milieu is exacerbated by endothelial glycocalyx degradation and upregulated adhesion molecules, which promote immune cell migration across the endothelium [7]. Disrupted EC chirality due to physical contact changed the intercellular junctions and increased endothelial permeability [44, 45]. Systemic inflammation-induced endothelial barrier dysfunction leads to interstitial fluid accumulation and elevated pressure, potentially compromising drug delivery and distribution [46]. Beyond maintaining vascular integrity, ECs exhibit innate immune capabilities, expressing a variety of receptors including Toll-like receptors (TLRs), NOD-like receptors (NLRs), and immune checkpoint receptors such as programmed cell death-ligand 1 (PD-L1) in response to inflammatory stimuli [20, 47-49]. Additionally, STING in ECs regulates T-cell adhesion and transendothelial migration *via* type 1 interferon [20].

In a murine model of psoriasis, YXKL treatment significantly decreased M1 macrophage/Th17 cell infiltration as well as lesional vascular density, while enhancing endothelial ZO-1 expression. However, the dose-dependent dissociation between CD31 inhibition (maximal at 3.64 g·kg^{-1}) and *α*-SMA response (observed only at 1.82 g·kg^{-1}) suggested that low-dose YXKL permits pericyte recruitment while partially suppressing angiogenesis, whereas high-dose YXKL actively prunes STING-high neovessels. This aligns with clinical evidence that excessive antiangiogenesis may hinder vascular normalization opportunities [50]. Our findings demonstrate that kaempferol and quercetin exert STING-dependent effects on angiogenesis and endothelial barrier integrity, but their immunomodulatory functions in ECs require further investigation. Kaempferol and quercetin suppressed M5-induced STING protein expression in HUVECs along with downstream IRF3 and NF-κB p65 activation, but they did not directly influence STING activation status itself. This suggests that for vascular remodeling in psoriasis, these compounds likely act through modulating STING expression or downstream signaling pathways rather than directly interfering with STING activation. The dissociation between STING protein suppression and unchanged activation state implies a more complex regulatory mechanism underlying their therapeutic effects.

This complexity arises because STING pathway activation is regulated by diverse mechanisms and factors. Beyond canonical cGAS activation, ataxia telangiectasia mutated (ATM) and interferon gamma-inducible protein 16 (IFI16) can induce TRAF6-mediated K63 ubiquitination of STING to activate NF-κB [33]. Conversely, cGAMP-induced AMPK-ULK1 phosphorylates STING at S366, negatively regulating the STING-IRF3 pathway [32]. Additional layers include Golgi-synthesized sulfated glycosaminoglycans modulating STING activation intensity [51] and adaptor protein complex 1 (AP-1)/clathrin complexes controlling signal termination [52]. Human STING exhibits heterogeneity, with varying expression levels of different alleles. The STING HAQ allele severely impairs over 90% of IFN-β secretion [53]. The F269S mutation causes ligand-independent interferon responses and exacerbates endothelial activation [54]. Although our study demonstrated that YXKL inhibits the activation of the STING/NF-κB pathway in psoriatic lesions, the multi-component nature suggests the presence of other components that may be involved in the regulation of STING signaling. However, our examination of key signaling molecules (TRAF6, AMPK, LKB1, ULK1) did not reveal significant regulation. Given that STING activation in psoriasis is primarily triggered by cytosolic DNA from cells damaged in the inflammatory microenvironment, interventions that protect cellular integrity or dampen broad inflammation might complement direct STING inhibition. In line with this, other bioactive components in YXKL, such as astilbin, which mitigates reactive oxygen species (ROS) accumulation and mitochondrial damage to reduce cytosolic DNA and cGAS-STING activation [55, 56]; eriodictyol, which alleviates endoplasmic reticulum stress to suppress keratinocyte inflammation [57]; and taxifolin, which reduces Th17 cell proportion by inhibiting JAK2/STAT3 signaling [38], could act synergistically or complementarily to contribute to the overall therapeutic effect. Our findings also open a transformative research path. Exploring the combination of YXKL with biologics that target downstream cytokines of the STING pathway, such as IL-17A. It represents a promising and clinically relevant direction and will offer valuable insights into rational drug combinations for enhanced therapeut-

ic outcomes.

Regrettably, we did not have the opportunity to use STING-deficient/overexpression mice for *in vivo* validation, nor could we rule out the possibility that patients with different STING alleles might respond differently to treatment. To establish causality and explore the impact of genetic heterogeneity, future studies should employ tissue-specific STING knockout/overexpression models and clinical cohort studies correlating STING genotypes with treatment response. Furthermore, the current lack of widely accepted methods to selectively activate the STING-NF-κB pathway without involving IRF3 presents a fundamental challenge not only for our work but for the entire field of STING biology. Developing specific STING-NF-κB agonists and elucidating precise activation mechanisms are crucial for advancing STING biology and developing targeted therapies. Such tools will significantly improve the validation and refinement of STING pathway modulation studies. In addition, although kaempferol and quercetin were identified as STING inhibitors, the binding characterization requires refinement. DARTS/CETSA confirmed physiological binding (10 μmol·L^{-1}), but MST-derived K_d values may underestimate affinity due to technical constraints. The cellular environment may enhance target binding through cofactor interactions. Future studies should employ SPR, point mutation, and co-crystal structure analysis to better identify the specific binding of kaempferol and quercetin to STING. Additionally, lipid-embedded STING preparations and evaluations of binding kinetics in endothelial cell membranes could provide more accurate models of the vascular context where these compounds exert their therapeutic effects.

5. Conclusion

Our study reveals the different dominant roles of the STING-IRF3 and STING/NF-κB pathways during psoriasis progression. This dynamic regulation may potentially represent a therapeutic strategy that could take effect both in the early stages of the disease and for maintaining long-term efficacy. The TCM formula, YXKL, exerts therapeutic effects by inhibiting activation of the STING/NF-κB pathway, which in turn reduces skin inflammatory damage and promotes vascular remodeling. Kaempferol and quercetin are the flavonoid components in YXKL with STING inhibitory activity; they bind to STING to suppress downstream pathway activation, leading to anti-inflammatory effects, inhibition of angiogenesis, and restoration of endothelial barrier function.

Funding

The work was supported by the Natural Science Foundation of Jiangsu Province (No. BK20220738), the CACMS Innovation Fund (No. CI2023C041LH), and the National Natural Science Foundation of China (Nos. 82304900 and 82274150).

Supporting information

The datasets used during the current study are available from the corresponding author upon reasonable request.

Declaration of competing interest

The authors have no conflict of interest.

Acknowledgments

We acknowledge Dr. Ruili Zhang at the Second Affiliated Hospital of Nanjing Medical University for assessing the severity of patients and collecting samples.

References

1 Griffiths C, Armstrong AW, Gudjonsson JE, et al. Psoriasis. *Lancet*. 2021;397 (10281):1301-1315. https://doi.org/10.1016/S0140-6736(20)32549-6.
2 Yu J, Zhao Q, Wang X, et al. Pathogenesis, multi-omics research, and clinical treatment of psoriasis. *J Autoimmun*. 2022;133:102916. https://doi.org/10.1016/j.jaut.2022.102916.
3 Svedbom A, Mallbris L, González-Cantero Á, et al. Skin inflammation, systemic inflammation, and cardiovascular disease in psoriasis. *JAMA Dermatol*. 2025;161(1):81-86. https://doi.org/10.1001/jamadermatol.2024.4433.
4 Markham T, Mullan R, Golden-Mason L, et al. Resolution of endothelial activation and down-regulation of Tie2 receptor in psoriatic skin after infliximab therapy. *J Am Acad Dermatol*. 2006;54(6):1003-1012. https://doi.org/10.1016/j.jaad.2006.01.038.
5 Hanssen S, van der Vleuten C, van Erp P, et al. The effect of adalimumab on the vasculature in psoriatic skin lesions. *J Dermatolog Treat*. 2019;30(3):221-226. https://doi.org/10.1080/09546634.2018.1506082.
6 Chokshi A, Demory BM, Laloo A, et al. Paradoxical tumor necrosis factor-alpha (TNF-α) inhibitor-induced psoriasis: a systematic review of pathogenesis, clinical presentation, and treatment. *Cureus*. 2023;15(8): e42791. https://doi.org/10.7759/cureus.42791.
7 Li Q, Shao S, Zhu Z, et al. An IGFBP7hi endothelial cell subset drives T cell extravasation in psoriasis *via* endothelial glycocalyx degradation. *J Clin Invest*. 2023;133(9):e160451. https://doi.org/10.1172/JCI160451.
8 Xie X, Cui Q, Jiang T, et al. A critical role of the endothelial S-phase kinase-associated protein 2/phosphatase and tensin homologue axis in angiogenesis and psoriasis. *Br J Dermatol*. 2024;190(2):244-257. https://doi.org/10.1093/bjd/ljad399.
9 Vestweber D. VE-cadherin: the major endothelial adhesion molecule controlling cellular junctions and blood vessel formation. *Arterioscler Thromb Vasc Biol*. 2008;28(2):223-232. https://doi.org/10.1161/ATVBAHA.107.158014.
10 Mikelis CM, Simaan M, Ando K, et al. RhoA and ROCK mediate histamine-induced vascular leakage and anaphylactic shock. *Nat Commun*. 2015;6:6725. https://doi.org/10.1038/ncomms7725.
11 Schonthaler HB, Huggenberger R, Wculek SK, et al. Systemic anti-VEGF treatment strongly reduces skin inflammation in a mouse model of psoriasis. *Proc Natl Acad Sci U S A*. 2009;106(50):21264-21269. https://doi.org/10.1073/pnas.0907550106.
12 Zhang B, Mei J, Liao Q, et al. Multitranscriptome analysis reveals stromal cells in the papillary dermis to promote angiogenesis in psoriasis vulgaris. *Br J Dermatol*. 2025;192(4):672-683. https://doi.org/10.1093/bjd/ljae459.
13 Yamamoto S, Niida S, Azuma E, et al. Inflammation-induced endothelial cell-derived extracellular vesicles modulate the cellular status of pericytes. *Sci Rep*. 2015;5:8505. https://doi.org/10.1038/srep08505.
14 Pan Y, You Y, Sun L, et al. The STING antagonist H-151 ameliorates psoriasis *via* suppression of STING/NF-κB-mediated inflammation. *Br J Pharmacol*. 2021;178(24):4907-4922. https://doi.org/10.1111/bph.15673.
15 Yu Y, Xue X, Tang W, et al. Cytosolic DNA-mediated STING-dependent inflammation contributes to the progression of psoriasis. *J Invest Dermatol*. 2021;142(3 Pt B):898-906.e4. https://doi.org/10.1016/j.jid.2021.08.430.
16 Sun X, Liu L, Wang J, et al. Targeting STING in dendritic cells alleviates psoriatic inflammation by suppressing IL-17A production. *Cell Mol Immunol*. 2024;21(7):738-751. https://doi.org/10.1038/s41423-024-01160-y.
17 Beranek M, Fiala Z, Kremlacek J, et al. Changes in circulating cell-free DNA and nucleosomes in patients with exacerbated psoriasis. *Arch Dermatol Res*. 2017;309(10):815-821. https://doi.org/10.1007/s00403-017-1785-5.
18 Ablasser A, Schmid-Burgk JL, Hemmerling I, et al. Cell intrinsic immunity spreads to bystander cells *via* the intercellular transfer of cGAMP. *Nature*. 2013;503(7477):530-534. https://doi.org/10.1038/nature12640.
19 Chiliveru S, Rahbek SH, Jensen SK, et al. Inflammatory cytokines break down intrinsic immunological tolerance of human primary keratinocytes to cytosolic DNA. *J Immunol*. 2014;192(5):2395-2404. https://doi.org/10.4049/jimmunol.1302120.
20 Anastasiou M, Newton GA, Kaur K, et al. Endothelial STING controls T cell transmigration in an IFNI-dependent manner. *JCI Insight*. 2021;6(15): e149346. https://doi.org/10.1172/jci.insight.149346.
21 Ma X, Wu W, Liang W, et al. Modulation of cGAS-STING signaling by PPARα in a mouse model of ischemia-induced retinopathy. *Proc Natl Acad Sci U S A*. 2022;119(48):e2208934119. https://doi.org/10.1073/pnas.2208934119.
22 Ni B, Yang Z, Zhou T, et al. Therapeutic intervention in neuroinflammation for neovascular ocular diseases through targeting the cGAS-STING-necroptosis pathway. *J Neuroinflammation*. 2024;21(1):164. https://doi.org/10.1186/s12974-024-03155-y.
23 Committee on Psoriasis, Chinese Society of Dermatology. Guideline for the diagnosis and treatment of psoriasis in China (2018 complete edition). *Chin J Dermatol*. 2019;52(10):667-710. https://doi.org/10.35541/cjd.20190847.
24 Su D, Zhang X, Zhang L, et al. A randomized, double-blind, controlled clinical study on the curative effect of huaier on mild-to-moderate psoriasis and an experimental study on the proliferation of hacat cells. *Biomed Res Int*. 2018;2018:2372895. https://doi.org/10.1155/2018/2372895.
25 Liang G, Nie Y, Chang Y, et al. Protective effects of Rhizoma Smilacis Glabrae extracts on potassium oxonate- and monosodium urate-induced hyperuricemia and gout in mice. *Phytomedicine*. 2019;59:152772. https://doi.org/10.1016/j.phymed.2018.11.032.
26 Feng H, He Y, La L, et al. The flavonoid-enriched extract from the root of *Smilax china* L. inhibits inflammatory responses *via* the TLR-4-mediated signaling pathway. *J Ethnopharmacol*. 2020;256:112785. https://doi.org/10.1016/j.jep.2020.112785.
27 Tang Y, Yu J, Zhao W, et al. Total glucosides of Rhizoma Smilacis Glabrae: a

therapeutic approach for psoriasis by regulating Th17/Treg balance. *Chin J Nat Med*. 2023;21(8):589-598. https://doi.org/10.1016/s1875-5364(23)60413-3.
28 Kim J, Bissonnette R, Lee J, et al. The spectrum of mild to severe psoriasis vulgaris is defined by a common activation of IL-17 pathway genes, but with key differences in immune regulatory genes. *J Invest Dermatol*. 2016;136(11):2173-2182. https://doi.org/10.1016/j.jid.2016.04.032.
29 Kim J, Oh CH, Jeon J, et al. Molecular phenotyping small (Asian) versus large (Western) plaque psoriasis shows common activation of IL-17 pathway genes but different regulatory gene sets. *J Invest Dermatol*. 2016;136(1):161-172. https://doi.org/10.1038/JID.2015.378.
30 Lu Y, Qi Y, Li L, et al. The gene expression analysis of peripheral blood monocytes from psoriasis vulgaris patients with different traditional Chinese medicine syndromes. *Front Pharmacol*. 2021;12:759741. https://doi.org/10.3389/fphar.2021.759741.
31 Shannon P, Markiel A, Ozier O, et al. Cytoscape: a software environment for integrated models of biomolecular interaction networks. *Genome Res*. 2003;13(11):2498-2504. https://doi.org/10.1101/gr.1239303.
32 Konno H, Konno K, Barber GN. Cyclic dinucleotides trigger ULK1 (ATG1) phosphorylation of STING to prevent sustained innate immune signaling. *Cell*. 2013;155(3):688-698. https://doi.org/10.1016/j.cell.2013.09.049.
33 Dunphy G, Flannery SM, Almine JF, et al. Non-canonical activation of the DNA sensing adaptor STING by ATM and IFI16 mediates NF-κB signaling after nuclear DNA damage. *Mol Cell*. 2018;71(5):745-760.e5. https://doi.org/10.1016/j.molcel.2018.07.034.
34 Siu T, Altman MD, Baltus GA, et al. Discovery of a novel cGAMP competitive ligand of the inactive form of STING. *ACS Med Chem Lett*. 2019;10(1):92-97. https://doi.org/10.1021/acsmedchemlett.8b00466.
35 Andres-Ejarque R, Ale HB, Grys K, et al. Enhanced NF-κB signaling in type-2 dendritic cells at baseline predicts non-response to adalimumab in psoriasis. *Nat Commun*. 2021;12(1):4741. https://doi.org/10.1038/s41467-021-25066-9.
36 Saggini A, Chimenti S, Chiricozzi A. IL-6 as a druggable target in psoriasis: focus on pustular variants. *J Immunol Res*. 2014;2014:964069. https://doi.org/10.1155/2014/964069.
37 Blauvelt A. IL-6 differs from TNF-α: unpredicted clinical effects caused by IL-6 blockade in psoriasis. *J Invest Dermatol*. 2017;137(3):541-542. https://doi.org/10.1016/j.jid.2016.11.022.
38 Yuan X, Li N, Zhang M, et al. Taxifolin attenuates IMQ-induced murine psoriasis-like dermatitis by regulating T helper cell responses *via* Notch1 and JAK2/STAT3 signal pathways. *Biomed Pharmacother*. 2020;123:109747. https://doi.org/10.1016/j.biopha.2019.109747.
39 Gupta SC, Phromnoi K, Aggarwal BB. Morin inhibits STAT3 tyrosine 705 phosphorylation in tumor cells through activation of protein tyrosine phosphatase SHP1. *Biochem Pharmacol*. 2013;85(7):898-912. https://doi.org/10.1016/j.bcp.2012.12.018.
40 McGeachy MJ, Bak-Jensen KS, Chen Y, et al. TGF-beta and IL-6 drive the production of IL-17 and IL-10 by T cells and restrain T(H)-17 cell-mediated pathology. *Nat Immunol*. 2007;8(12):1390-1397. https://doi.org/10.1038/ni1539.
41 Zhou L, Ivanov II, Spolski R, et al. IL-6 programs T(H)-17 cell differentiation by promoting sequential engagement of the IL-21 and IL-23 pathways. *Nat Immunol*. 2007;8:967-974. https://doi.org/10.1038/ni1488.
42 Wu D, Hailer AA, Wang S, et al. A single-cell atlas of IL-23 inhibition in cutaneous psoriasis distinguishes clinical response. *Sci Immunol*. 2024;9(91):eadi2848. https://doi.org/10.1126/sciimmunol.adi2848.
43 Lou F, Sun Y, Xu Z, et al. Excessive polyamine generation in keratinocytes promotes self-RNA sensing by dendritic cells in psoriasis. *Immunity*. 2020;53(1):204-216.e10. https://doi.org/10.1016/j.immuni.2020.06.004.
44 Fan J, Ray P, Lu YW, et al. Cell chirality regulates intercellular junctions and endothelial permeability. *Sci Adv*. 2018;4(10):eaat2111. https://doi.org/10.1126/sciadv.aat2111.
45 Hang B, Jassem E, Mohammed H, et al. Interacting with tumor cells weakens the intrinsic clockwise chirality of endothelial cells. *APL Bioeng*. 2022;6(4):046107. https://doi.org/10.1063/5.0115827.
46 Dwairy M, Reddy JN, Righetti R. Predicting stress and interstitial fluid pressure in tumors based on biphasic theory. *Comput Biol Med*. 2023;167:107651. https://doi.org/10.1016/j.compbiomed.2023.107651.
47 Patten DA, Wilson GK, Bailey D, et al. Human liver sinusoidal endothelial cells promote intracellular crawling of lymphocytes during recruitment: a new step in migration. *Hepatology*. 2017;65(1):294-309. https://doi.org/10.1002/hep.28879.
48 Shao Y, Saredy J, Yang WY, et al. Vascular endothelial cells and innate immunity. *Arterioscler Thromb Vasc Biol*. 2020;40(6):e138-e152. https://doi.org/10.1161/ATVBAHA.120.314330.
49 Fu Y, Gong T, Loughran PA, et al. Roles of TLR4 in macrophage immunity and macrophage-pulmonary vascular/lymphatic endothelial cell interactions in sepsis. *Commun Biol*. 2025;8(1):469. https://doi.org/10.1038/s42003-025-07921-3.
50 Jain RK, Duda DG, Clark JW, et al. Lessons from phase III clinical trials on anti-VEGF therapy for cancer. *Nat Clin Pract Oncol*. 2006;3(1):24-40. https://doi.org/10.1038/ncponc0403.
51 Fang R, Jiang Q, Guan Y, et al. Golgi apparatus-synthesized sulfated glycosaminoglycans mediate polymerization and activation of the cGAMP sensor STING. *Immunity*. 2021;54(5):962-975.e8. https://doi.org/10.1016/j.immuni.2021.03.011.
52 Liu Y, Xu P, Rivara S, et al. Clathrin-associated AP-1 controls termination of STING signalling. *Nature*. 2022;610(7933):761-767. https://doi.org/10.1038/s41586-022-05354-0.
53 Patel S, Blaauboer SM, Tucker HR, et al. The common R71H-G230A-R293Q human TMEM173 is a null allele. *J Immunol*. 2017;198(2):776-787. https://doi.org/10.4049/jimmunol.1601585.
54 Valeri E, Breggion S, Barzaghi F, et al. A novel STING variant triggers endothelial toxicity and SAVI disease. *J Exp Med*. 2024;221(9):e20232167. https://doi.org/10.1084/jem.20232167.
55 Xu X, Zhang H, Chang A, et al. Astilbin alleviates IL-17-induced hyperproliferation and inflammation in HaCaT cells *via* inhibiting ferroptosis through the cGAS-STING pathway. *Int J Mol Sci*. 2025;26(11):5075. https://doi.org/10.3390/ijms26115075.
56 Wang W, Yuhai, Wang H, et al. Astilbin reduces ROS accumulation and VEGF expression through Nrf2 in psoriasis-like skin disease. *Biol Res*. 2019;52(1):49. https://doi.org/10.1186/s40659-019-0255-2.
57 Yuan R, Sun QC, An YP, et al. Eriodictyol inhibits the proliferation and inflammatory response in keratinocytes in psoriasis through inactivating DYRK1A-mediated endoplasmic reticulum stress. *J Asian Nat Prod Res*. 2025;27(7):1025-1037. https://doi.org/10.1080/10286020.2024.2446301.